CANCER RESEARCH COMMUNICATIONS

AACR American Association for Cancer Research

RESEARCH ARTICLE https://aacrjournals.org/10.1158/2767-9764.CRC-21-0106 OPEN ACCESS

Tumor Suppressor PLK2 May Serve as a Biomarker in Triple-Negative Breast Cancer for Improved Response to PLK1 Therapeutics

Yang Gao[1,2,3], Elena B. Kabotyanski[1,2], Jonathan H. Shepherd[4], Elizabeth Villegas[5], Deanna Acosta[1,2], Clark Hamor[1,2], Tingting Sun[2,6,7], Celina Montmeyor-Garcia[8], Xiaping He[4], Lacey E. Dobrolecki[1,2,3], Thomas F. Westbrook[2,6,7], Michael T. Lewis[1,2,3], Susan G. Hilsenbeck[2,3], Xiang H.-F. Zhang[1,2,3,9], Charles M. Perou[4], and Jeffrey M. Rosen[1,2]

ABSTRACT

Polo-like kinase (PLK) family members play important roles in cell-cycle regulation. The founding member PLK1 is oncogenic and preclinically validated as a cancer therapeutic target. Paradoxically, frequent loss of chromosome 5q11–35, which includes PLK2, is observed in basal-like breast cancer. In this study, we found that PLK2 was tumor suppressive in breast cancer, preferentially in basal-like and triple-negative breast cancer (TNBC) subtypes. Knockdown of PLK1 rescued phenotypes induced by PLK2 loss both *in vitro* and *in vivo*. We also demonstrated that PLK2 directly interacted with PLK1 at prometaphase through the kinase but not the polo-box domains of PLK2, suggesting PLK2 functioned at least partially through the interaction with PLK1. Furthermore, an improved treatment response was seen in both Plk2-deleted/low mouse preclinical and patient-derived xenograft (PDX) TNBC models using the PLK1 inhibitor volasertib alone or in combination with carboplatin. Reexpression of PLK2 in an inducible PLK2-null mouse model reduced the therapeutic efficacy of volasertib. In summary, this study delineates the effects of chromosome 5q loss in TNBC that includes PLK2, the relationship between PLK2 and PLK1, and how this may render PLK2-deleted/low tumors more sensitive to PLK1 inhibition in combination with chemotherapy.

Significance: The tumor-suppressive role of PLK2, and its relationship with oncogene *PLK1*, provide a mechanistic rationalization to use PLK1 inhibitors in combination with chemotherapy to treat PLK2-low/deleted tumors. TNBC, and other cancers with low PLK2 expression, are such candidates to leverage precision medicine to identify patients who might benefit from treatment with these inhibitors.

Introduction

Breast cancer remains the most prevalent cancer and the second leading cause of cancer-related death in American women in 2021 (1). Therefore, it is imperative to understand the molecular mechanisms underlying breast cancer development in order to develop novel therapies. Categorization of breast cancer based on its status of estrogen receptor (ER), progesterone receptor (PR), and HER2 has markedly improved the treatment of the luminal and HER2-specific subtypes (2, 3). For example, the luminal subtype (ER^+, $PR^{\pm}$) typically responds to endocrine therapies, and the HER2 subtype ($HER2^+$, $ER^{-/+}$, $PR^{-/+}$) is treated with the HER2-targeted drug trastuzumab (4–8). However, targeted therapies are still in urgent need for triple-negative breast cancer (TNBC, ER^-, PR^-, and $HER2^-$) due to the lack of these standard therapeutic targets. In this study, we identified a potent candidate biomarker, Polo-like kinase 2 (PLK2, chromosome 5q11.2), and a possible therapeutic target PLK1, that may not only help stratify patients with TNBC for treatment, but also benefit for patients with other cancers that exhibit chromosome 5q loss across the PLK2 region (9, 10).

PLK2 belongs to a gene family consisting of five serine/threonine kinases (PLK1-PLK5) with highly conserved N-terminal kinase domains and C-terminal polo-box domains (PBD). PLK family members play important roles in regulating the cell cycle and DNA damage response (11–13). The founding and most well-studied member of the family, PLK1, is expressed in the proliferating cells of normal tissues with a peak during G_2/M and controls many

[1]Department of Molecular and Cellular Biology, Baylor College of Medicine, Houston, Texas. [2]Dan L. Duncan Cancer Center, Baylor College of Medicine, Houston, Texas. [3]Lester and Sue Smith Breast Center, Baylor College of Medicine, Houston, Texas. [4]The University of North Carolina at Chapel Hill, Chapel Hill, North Carolina. [5]University of Houston-Downtown, Houston, Texas. [6]Department of Molecular and Human Genetics, Baylor College of Medicine, Houston, Texas. [7]Verna & Marrs McLean Department of Biochemistry and Molecular Biology, Baylor College of Medicine, Houston, Texas. [8]Canadian Blood Services, Toronto, Ontario, Canada. [9]McNair Medical Institute, Baylor College of Medicine, Houston, Texas.

Current address for T. Sun: Bristol Myers Squibb, Seattle, Washington.

Corresponding Author: Jeffrey M. Rosen, Baylor College of Medicine, 1 Baylor Plaza, Houston, TX 77030. Phone: 832-215-9503; E-mail: jrosen@bcm.edu

doi: 10.1158/2767-9764.CRC-21-0106

cell-cycle events including centrosome maturation, mitotic entry, chromosome segregation, and cytokinesis (13–15). Extensive studies have shown that PLK1 overexpression is oncogenic in many types of cancer and it has been validated preclinically as a cancer therapeutic target (16–18). Several PLK1 inhibitors, such as volasertib (BI 6727; ref. 19), are currently under clinical development. PLK1 inhibition in combination with paclitaxel, or doxorubicin plus cyclophosphamide, achieved a better outcome in the treatment of TNBC xenograft models (20, 21). Volasertib plus carboplatin has demonstrated activity in heavily pretreated patients with advanced solid tumors, including breast tumor (22).

PLK2 was initially named serum-inducible kinase (SNK) because it is an early growth response gene upon serum treatment (23). PLK2 is mainly localized in centrosomes during the G_1 phase and is necessary for centriole duplication (24–26). It also functions in the nervous system by regulating homeostatic synaptic plasticity and neuronal cell differentiation (13, 27, 28). Plk2-null mice display embryonic growth retardation but are viable, which may be due to compensatory effects of other Plks (29). PLK2 is highly expressed in the mammary gland (30). In contrast to *in vitro* studies, deletion of Plk2 in mouse mammary epithelial cells (MEC) *in vivo* surprisingly not only induces cell proliferation and gland hyperbranching, but also disrupts mitotic spindle orientation and cellular polarity (31). Moreover, loss of Plk2 results in an increased number of less differentiated preneoplastic lesions in the mammary glands of multiparous mice, suggesting PLK2 is required for normal mammary gland development (31).

Although PLK2 belongs to the same family as PLK1, and both kinases are implicated in cell-cycle progression, recent studies as well as our data presented herein suggest that PLK2 may actually be a tumor suppressor that is silenced in many types of cancers, including breast cancer (32–36). This paradox stimulated us to investigate the functions of PLK1 and PLK2 in breast cancer, as well as potential translational implications. Here, we demonstrated that PLK2 functions as a tumor suppressor in breast cancer, and suggested that its tumor-suppressive role is mediated, at least partially, by its direct interaction with PLK1. Furthermore, using both preclinical genetically engineered mouse (GEM) models and patient-derived xenograft (PDX) models, we showed that PLK2 loss may serve as a potential biomarker to predict response to PLK1 inhibitors, alone and in combination with chemotherapy.

Materials and Methods

Cell Culture

HEK293T and BT20 cells were purchased from ATCC in 2012 and 2013, respectively. They have not been authenticated since the purchase. They were cultured in DMEM/High Glucose medium (GenDepot) supplemented with 10% FBS plus antibiotic–antimycotic solution (GenDepot). TLM-HMECs (genetically engineered human mammary epithelial cells) have not been authenticated since they were obtained from Dr. Thomas Roberts (Dana-Farber Cancer Institute, Harvard Medical School, Boston, MA) in 2003 (37) and were cultured in mammary epithelial growth medium (MEGM, Lonza). All cell lines used in this study were grown in a humidified incubator at 37°C with 5% CO_2 and *Mycoplasma* free as periodically tested by Universal Mycoplasma Detection Kit (ATCC).

Anchorage-Independent Proliferation Assay

TLM-HMECs were lentivirally transduced with control or human PLK2 GIPZ lentiviral short hairpin RNAs (shRNA; Open Biosystems-Horizon Discovery; Supplementary Table S3), and then selected using puromycin to establish stable cell lines. These cell lines were subsequently transduced with lentiviruses expressing control or human PLK1 GIPZ lentiviral shRNA (Open Biosystems-Horizon Discovery; Supplementary Table S3), at a multiplicity of infection (MOI) of 1 and subjected to anchorage-independent proliferation assays as described previously (38). Cells were seeded at densities of 3×10^4 or 5×10^4 per 60-mm plate with a bottom layer of 0.6% Noble agar in MEM (Gibco) and a top layer of 0.5% methylcellulose containing MEGM (Lonza). Fresh MEGM (0.5 mL) was added every three days. Macroscopic colonies were counted after four weeks. Experiments were performed in triplicate.

Primary Mammary Epithelial Cell Isolation, Transduction, and Transplantation

Primary mammary epithelial cells (MEC) were isolated from 8-week-old $Plk2^{-/-}$ mice for transplantation experiments. MECs were isolated by mincing freshly harvested mammary glands into 1 mm^3 fragments using a Vibratome Series 800-Mcllwain Tissue Chopper. The tissue fragments were digested in DMEM/F12, which contained 2 mg/mL collagenase A (Roche Applied Science), for 1 hour at 37°C shaking at 120 rpm. The adipocytes were removed from the organoids by centrifugation at 1,500 rpm for 5 minutes. Following this centrifugation step, the remaining stromal cells were removed by sequential centrifugation at 1,500 rpm for 5 seconds. The organoids were then subjected to trypsinization by resuspending them in 0.25% Trypsin-EDTA for 5 minutes at 37°C and subsequently the organoids were washed and filtered using a 40-μm cell strainer to obtain a single-cell suspension.

A LeGO-T lentiviral vector was kindly provided by Kristoffer Riecken (39). shRNAs targeting mouse Plk1 (Supplementary Table S3) were purchased from Open Biosystems-Horizon Discovery. U6 promoter-hairpin segments were amplified from a pLKO.1 vector using PCR primers *Xba*I (forward): gagatctagaccttcaccgagggcctatttc; and *Not*I (reverse): gagagcggccgcccatttgtctcgaggtcgag. Both LeGO-T lentiviral vector and PCR fragments were digested with *Xba*I + *Not*I, purified with QIAquick Gel Extraction kit or QIAquick PCR Purification kit (Qiagen), ligated using T4 DNA Ligase (New England BioLabs), and transformed into One Shot Stbl3-competent cells (Life Technologies). All plasmids were sequence-verified prior to lentiviral production. Lentiviral vectors were cotransfected with packaging vectors VSVG and gag/pol in a ratio of 3:1:2 into HEK293T cells using Trans-IT Transfection reagent (Mirus). Viral supernatants were collected at 48 and 72 hours posttransfection, pooled, and filtered through 0.45-μm filters to remove cellular debris. Filtered viral supernatants were concentrated using Beckman Coulter Optima ultracentrifuge (SW32Ti rotor) at 25,000 rpm for 1 hour 45 minutes. Ultracentrifuged viruses were resuspended in MEC growth media and titered by FACS analysis as described before (40).

Primary MECs were plated in a nonadherent dish and were transduced with the above lentiviral Plk1 at an MOI of 50. Cells were incubated at 37°C overnight. The next day, cells were washed to remove any unbound virus and were resuspended in DMEM/F12 containing 20% Matrigel and kept on ice until transplantation. For transplants, 150,000 cells were injected into cleared contralateral fat pads of 3-week-old SCID/Beige host mice. Mammary glands were harvested 8 weeks posttransplantation and whole-mount, as well as histologic analyses, were performed.

Estrogen and Progesterone Treatment

To induce proliferation in mammary epithelial cells and quantify the mitotic spindle orientation, mice were treated with estrogen and progesterone for two

days as described previously (31). In brief, mice were injected with 100 μL of estrogen and progesterone sesame oil solution with a final concentration of 1 μg of E2 and 1 mg of progesterone under the skin between the shoulder blades.

Tissue Harvest

The fourth pair of mammary glands was harvested at 8 weeks posttransplantation. Bromodeoxyuridine (BrdU) (B5002, Sigma-Aldrich) at 60 μg/g body weight was intraperitoneally injected 2 hours prior to tissue harvest, which allowed for proliferation analysis.

RNA Isolation

The fourth pair of mammary glands was isolated and MECs were purified from these glands. Total RNA was isolated using TRIzol Reagent (Invitrogen) or RNeasy Mini Kit (Qiagen) according to the manufacturer's protocols. Similar RNA preparations were also done for the tumor samples.

Protein Extraction and Immunoblot Analysis

Protein was isolated using RIPA Lysis and Extraction Buffer (Thermo Scientific) or T-PER Tissue Protein Extraction Buffer (Thermo Scientific) plus protease inhibitor (Roche) and phosphatase inhibitor (Roche). Protein was quantified using a Pierce BCA Protein Assay Kit (Thermo Scientific). SDS-PAGE was employed to separate proteins that were transferred onto a polyvinylidene difluoride membrane. PLK1 (Abcam, ab17057, 1:1,000), PLK2 (Cell Signaling Technology, 14821, 1:1,000), GAPDH (Cell Signaling Technology, 2118, 1:5,000), and β-actin (Cell Signaling Technology, 3700, 1:3,000) antibodies were used.

Whole-Mount, Carmine Alum Staining, and Branching Analysis

For mammary gland whole-mount analysis, tissue was mounted between two glass slides and imaged using Leica MZ16F fluorescence stereoscope. Images (1.0× and 1.6×) of control luciferase and Plk1 shRNA lentiviral vector-transduced mammary glands were taken for branching analysis. Following these analyses, mammary glands were paraffin-embedded. Carmine alum staining was performed as described previously (31).

Immunofluorescence

Paraffin-embedded tissues were cut into 5-μm–thick sections and dried before use. To begin, sections were deparaffinized in xylene and rehydrated in graded ethanol solutions. Antigen retrieval was performed by boiling in 10 nmol/L sodium citrate buffer (pH 6.0) for 20 minutes. Washing steps were performed with 1× PBS and primary antibodies were incubated at 4°C overnight in a humidified chamber. All primary antibodies (BrdU, Abcam, ab6326, 1:1,000; NuMA, Abcam, ab36999, 1:250) were diluted in 5% BSA, 0.5% Tween-20 blocking buffer.

Bimolecular Fluorescence Complementation Assay

pDONR vectors encoding PLK2, RB1, CHK1, TUBB, and PLK1 were obtained from human ORFeome (Open Biosystems-Horizon Discovery). They were individually transferred into either bait pB-CMV-CVn-neo (for PLK2) or prey pB-CMV-YFP-CC-puro (for RB1, TUBB, CHK1, PLK1) vectors using Gateway recombination reaction (Life Technologies; ref. 41). Bait and prey plasmids containing fused fragments were then individually transfected together with VSVG and gag/pol packaging vectors in a ratio of 3:1:1 into HEK293T cells using Trans-IT Transfection reagent (Mirus) to produce retroviruses. Stable cell lines were generated after selection with G418 (500 μg/mL; bait) and puromycin (2 μg/mL; prey), and the expression of proteins was verified by immunofluorescence and Western blotting. In bimolecular fluorescence complementation (BiFC) assay, the PLK2-bait cell line was infected with one of the CHEK1, TUBB, RB1, or PLK1 prey–produced retroviruses.

Fluorescent signals were observed after 48 hours of infection using a Carl Zeiss inverted fluorescence microscope with an AxioCam MRm camera. BD LSRII Flow Cytometer (BD Biosciences) was utilized to quantify yellow fluorescent protein (YFP)-positive cells. Untransduced cells, cells transduced with bait-empty vector (without PLK2 fusion), or cells transduced with only one expression vector containing a fused fragment (either bait or prey) were used as negative controls. BiFC assays were repeated five times in triplicates.

Proximity Ligation Assay

Full-length PLK1 and PLK2 sequences were PCR amplified and individually cloned into pCDNA3.1 vector (Invitrogen) using *Xba*I-*Eco*RI and *Xba*I-*Bam*HI (New England BioLabs) restriction sites, respectively. PLK2 mutations K111R (KD, kinase dead), W503F (PBD, polo-box domain 1) and H629A, K631M (PBD, polo-box domain 2) were generated by site-directed mutagenesis (Agilent Technologies) according to the manufacturer's protocol. All constructs were verified by DNA sequence analysis prior to transfections.

HEK293T cells were seeded at 40% confluence before the day of transfection. To induce an arrest in the G_2/M phase of the cell cycle, cells were treated with 40 ng/mL of nocodazole (Sigma-Aldrich) for 16 hours. For each transfection, 2.5 μg of total DNA was mixed with 250 μL of Opti-MEM I Reduced-Serum medium (Life Technologies) and 7.5 μL of Trans-IT-293 Reagent (Mirus). The mixture was incubated at room temperature for 20 minutes and then added to cells. After 48 hours, cells were transferred into a 96-well SensoPlate with a glass bottom (Thermo Scientific) in the amount of 10^4 cells per well and were grown for another 24 hours. Subsequently, cells were fixed with 4% paraformaldehyde (Thermo Scientific) for 10 minutes, permeabilized with 0.25% TritonX-100 for 10 minutes, and blocked with 3% BSA in PBS for 1 hour at room temperature. Then, cells were coincubated with mouse anti-PLK1 antibody (Abcam, ab17057) diluted 1:4,000 and rabbit anti-PLK2 antibody (Cell Signaling Technology, 14812) diluted 1:2,000 overnight at 4°C. The PLA was performed using reagents supplied in the Duolink in situ Red PLA Mouse/Rabbit kit (Sigma-Aldrich, DUO92101) following the manufacturer's instructions. Cell nuclei were stained with NucBlue ReadyProbes reagent (Invitrogen), and actin filaments were stained with Actin Green 488 ReadyProbes reagent (Invitrogen).

Imaging was performed on a Cytiva DV Live epifluorescence image restoration microscope using an Olympus PlanApo N 60×/1.42 NA objective and 1.9k × 1.9k pco.EDGE sCMOS_5.5 camera with 1042 × 1042 FOV. The filter sets used were DAPI (390/18 excitation, 435/48 emission) and CY5 (632/22 excitation, 676/34 emission). Z-stacks (0.25 μm) covering the whole cell (~8.3 μm) were acquired before applying a conservative restorative algorithm for quantitative image deconvolution using SoftWorx v7.0 and saving files in pixel intensity projection tiff format for each channel. Imaging for quantitation of PLA-positive cells was done on a BioTek Cytation 5 Cell Imaging Multi-Mode Reader equipped with a DAPI filter cube set (excitation 377/50, emission 447/60) and CY5 filter cube set (excitation 628/40, emission 685/40) with a Grasshopper3 GS3-U3–14S5M camera. Image panels were collected with an Olympus 20×/0.45NA objective. Images were exported from the Gen5 version 3.03.10 software as tiff files. Quantitative PLA analysis was performed by

calculating the percentage of cells showing positive PLA signals from eight randomly captured image panels per group.

RNA-sequencing and Bioinformatic Data Analyses

RNA-sequencing (RNA-seq) was performed as described previously (42). Briefly, paired-end (2 × 50 bp) sequencing was performed on the Illumina HiSeq 2500 sequencer at the UNC High Throughput Sequencing Facility. RNA-seq results were aligned to the mouse mm10 reference genome using the Star alignment algorithm (43) and quantified as gene-level counts using a Salmon pipeline as described previously (42). Upper-quartile normalized counts were then log2(x+1) transformed. Hierarchical clustering was performed with 1,910 intrinsic mouse genes using Cluster 3.0 with 1—Pearson correlation distance and centroid linkage (44).

To compare the gene expression of $Plk2^{-/-}$; $p53^{-/-}$ models with published mouse model gene expression classes derived from microarray expression, we combined the $\log_2(x+1)$ RNA-seq expression data with the expression data from microarray samples previously used to identify mouse mammary tumor expression classes (44). Batch effects due to expression type (RNA-seq vs. microarray) were adjusted using COMBAT (45). Expression class assignments from the initial publication (44) were retained for microarray samples. $Plk2^{-/-}$; $p53^{-/-}$ samples were assigned to three separate expression classes (PLK2-Luminal, PLK2-Basal, and PLK2-Claudin-low) based on the hierarchical clustering with RNA-seq samples.

PLK2 and PLK1 mRNA expression levels in PDX models were evaluated in the BCM PDX Portal (https://pdxportal.research.bcm.edu/).

Copy-number data for The Cancer Genome Atlas (TCGA) breast cancer samples were downloaded from cBioPortal (www.cbioportal.org) using the TCGA Firehose Legacy version. Copy-number variation was calculated using GISTIC 2.0 with values < -2 indicating a deletion event (potentially homozygous deletion); values < -1 indicating a loss (potentially a heterozygous deletion), values near 0 indicating diploid status, values > 1 indicating a gain, and values >2 indicating an amplification.

Generation of Doxycycline-Inducible Cell Lines and Cell Culture Conditions

To derive a cell line from the 1963B $Plk2^{-/-}$; $p53^{-/-}$ tumor model, a fresh tumor was harvested when it reached approximately 1 cm in diameter. The 1963B tumor was then minced into small 1–2 mm^3 pieces and digested with 1 mg/mL type I Collagenase (Roche) in DMEM/F12 for 2 hours in a 37°C incubator shaking at 125 rpm. After centrifugation at 1,500 rpm for 5 minutes, the pellet was resuspended in PBS and then three short centrifugations (1,500 rpm at 7 seconds) were performed to enrich the mammary epithelial organoids. Single cells were obtained by digestion in 0.25% Trypsin-EDTA for 5 minutes at 37°C. Because the p53-null mice have a neomycin resistance cassette, the 1963B cell line was generated using 500 μg/mL G418 (Sigma) selection for two weeks and then validated by pan-cytokeratin and cytokeratin 5 immunofluorescence staining.

Doxycycline-inducible vector pCW57.1 was obtained from Addgene (#41393). PLK2 in a pDONR223 vector was obtained from human ORFeome (Open Biosystems-Horizon Discovery) and was cloned into pCW57.1 using the Gateway recombination reaction (Life Technologies) and verified by sequencing prior to transfection. For viral production, the plasmid was transfected together with packaging plasmids CMV-VSVG, MDL-RRE, and RSV-REV in the ratio of (3:1:1:1) into HEK293T cells using Trans-IT transfection reagent (Mirus). Virus-rich supernatant was collected at 72 hours posttransfection, concentrated by ultracentrifugation at 25,000 rpm for 1 hour 45 minutes, and titered using lentivirus qPCR titer kit (ABM). 1963B cell line generated as above and BT20 cells were transduced with the virus at an MOI of 10 following puromycin selection (2 μg/mL) for 5 days.

Mice, Tumor Models, and Treatment

All animal experiments were conducted in accordance with a protocol (AN-504) approved by the Institutional Animal Care and Use Committee of Baylor College of Medicine (Houston, TX) and in compliance with all relevant ethical regulations regarding animal research.

To generate $Plk2^{-/-}$; $p53^{-/-}$ mice, $Plk2^{-/-}$ mice were first backcrossed with wild-type Balb/c mice for >5 generations and then bred with the $p53^{-/-}$ Balb/c mice. To get breast-specific tumors, MECs isolated from $Plk2^{-/-}$; $p53^{-/-}$ mice were transplanted into cleared fat pads of wild-type Balb/c recipients. Spontaneous tumors arose with a latency of eight months to more than a year and were characterized by histology, hematoxylin and eosin, immunofluorescence staining, and RNA-seq. Those tumors were cryopreserved as small chunks for later mammary fat pad implantation experiments as described before (46). PDX models were obtained from the Patient-Derived Xenograft and Advanced In Vivo Models Core at Baylor College of Medicine (Houston, TX). Balb/c mice were purchased from Envigo. NSG mice were purchased from the Jackson laboratory.

When tumor size became approximately 110–200 mm^3, animals were randomized into different treatment groups. Carboplatin (Sigma-Aldrich, C2538) was reconstituted in PBS and delivered once a week at a dosage of 25 mg/kg or 50 mg/kg by intraperitoneal injection. Volasertib (Selleckchem, S2235) was formulated in 0.1 N hydrochloric acid (vehicle) and administered once a week by oral gavage at a dosage of 25 mg/kg or 50 mg/kg. Tumor size was measured using a digital caliper twice a week.

Doxycycline-treated mice were supplied with 200 μg/mL doxycycline water when their tumors became palpable. Doxycycline water was changed twice a week.

Statistical Analysis

Statistical comparisons were performed with Excel (Microsoft Office 2016), Prism software (GraphPad Software, version 9.0), or R software (Version 4.0). Significance of differences between two groups was evaluated by unpaired two-tailed *t* test. Pairwise *t* tests with Bonferroni correction were used for comparison between TCGA TNBC subtypes. Multiple comparisons were analyzed using one-or two-way ANOVA followed by Tukey test. Comparison of $\log_2$ fold change of tumor volume was performed using linear contrast or two-way ANOVA. The specific statistical analysis for each figure was included in the figure legends.

Data Availability

RNA-seq and microarray data were uploaded to Gene Expression Omnibus (accession number GSE174683).

Results

PLK2 is Tumor Suppressive in Breast Cancer

Previous studies from our laboratory and others have suggested that there is a frequent arm-level loss of chromosome 5q region across different types of

cancer, including breast cancer, lung squamous cell carcinoma, and ovarian cancer (9, 10). To explore the gene-specific copy-number alterations (CNA) of PLK2 (chromosome 5q11.2), we analyzed the TCGA Pan-Cancer and Tumorscape datasets using the TCGA Copy Number Portal from the Broad Institute and confirmed that PLK2 is significantly deleted in several types of cancer, including breast cancer (Fig. 1A; Supplementary Fig. S1A). This result is consistent with our previous report that basal-like breast tumors have a frequent loss of chromosome 5q11–35 that typically included PLK2 and the checkpoint clamp loader component gene *RAD17* (47). To gain more insight into the CNAs in different breast cancer subtypes, we performed GISTIC analysis on TCGA breast tumors and discovered that the loss of PLK2 was identified in 21.8% of all patients with breast cancer (Fig. 1B). Among these, loss of PLK2 was found in 11.3% of ER^+, 24.4% of $HER2^+$, but markedly in 58% of TNBC patients. Similar to PLK2, loss of RAD17 was also observed at a higher level in TNBC (Fig. 1B).

We then examined mRNA expression in the TCGA database to further investigate the relationship between PLK2 and PLK1 in breast cancer. Patients with primary breast tumors had lower expression of PLK2 mRNA, but higher levels of PLK1 mRNA, relative to normal breast tissue (Fig. 1C and D). Further analysis indicated that lower expression of PLK2 and a higher level of PLK1 mRNA was specifically linked to the basal-like subtype or TNBC subtype (Fig. 1C and D; Supplementary Fig. S1B and S1C).

In support of the functional consequences of these human tumor findings, an unbiased RNAi-based forward genetic screen also identified PLK2 as one of the candidate tumor suppressors in breast cancer (Fig. 1E; refs. 37, 38). In brief, human mammary epithelial cells (HMEC) were immortalized by transducing with human telomerase catalytic subunit (hTERT) and SV40 large T-antigen (LT), hereby designated TLM-HMECs. These cells, however, need to be anchored to the extracellular matrix (ECM) to proliferate. Therefore, by applying an shRNA library that targeted all kinases and phosphatases to TLM-HMECs cultured in the absence of ECM, we were able to discover critical candidate genes involved in cell transformation (38), including PLK2. Subsequently, we performed a colony transformation assay and found that knockdown of PLK2 in TLM-HMECs using two different shRNAs, both increased the number of colonies as compared with controls (Fig. 1F; Supplementary Fig. S1D–F), consistent with the tumor-suppressive role of PLK2.

PLK1 Mediates PLK2 Loss–Induced Phenotypes

PLK1 is overexpressed in breast cancer, especially TNBC, and targeting PLK1 has been reported to impair TNBC growth (20, 48). The apparent paradox that PLK1 and PLK2 might exert opposite roles in breast cancer led us to study potential links between PLK2 and PLK1. First, we tested the effect of PLK1 knockdown using a human PLK1 shRNA in the TLM-HMEC colony transformation assay. Knockdown of PLK1 alone did not significantly change the number of colonies formed, but instead it mitigated the increased colony formation observed following PLK2 knockdown, thus suggesting that the tumor suppressive function of PLK2 is specifically related to PLK1 activity (Fig. 1F; Supplementary Fig. S1D).

Next, we sought to examine whether inhibition of PLK1 was able to rescue the phenotypes observed following PLK2 loss in the mouse mammary gland *in vivo*. We isolated MECs from 8-week-old $Plk2^{-/-}$ mice and transduced them with lentiviral vectors containing control, mouse mPlk1 #1, or mPlk1 #2 shRNA (Supplementary Fig. S2). The cells were then injected into immunocompromised mice with cleared mammary fat pads. Transplanted outgrowths were harvested and characterized 8 weeks posttransplantation (Fig. 2A). Visualization of the fluorescent whole mounts and carmine alum staining showed that, as expected, the control outgrowths had increased branching, a phenotype previously observed in the $Plk2^{-/-}$ mammary glands (31). Interestingly, the hyperbranched phenotype observed in the control appeared to be absent in the Plk1 knockdown outgrowths. Quantification of the branchpoints per millimeter of duct revealed that the controls had about 2 branchpoints per millimeter of duct, whereas both the mPlk1 #1 and mPlk1 #2 shRNA knockdown groups had about 1.4 branchpoints per millimeter, suggesting Plk1 knockdown alleviated the hyperbranching phenotype in $Plk2^{-/-}$ mammary gland (Fig. 2B).

Mammary gland ductal epithelial cells have very low levels of proliferation when female mice become mature and the mammary ducts reach the edge of the mammary fat pad. However, Plk2 inactivation in mammary ducts leads to hyperproliferation and disorientated mitotic spindle formation in luminal epithelial cells, which exhibited an angle greater than 10° to the basement membrane (31). Subsequent knockdown of Plk1 decreased the high level of proliferating epithelial cells (∼6% BrdU positive) to the level usually observed in ducts in mature mice (∼0.4% BrdU positive; Fig. 2C). In addition, when the mice were treated with estrogen and progesterone to induce proliferation, knockdown of Plk1 decreased the percentage of mitotic epithelial cells with misoriented mitotic spindles and increased the presence of mitotic cells with normal spindle orientation parallel to the basement membrane (Fig. 2D). These data suggest that the phenotypes associated with PLK2-loss are mediated, at least partially, by PLK1 during mammary gland development.

PLK2 Directly Interacts with PLK1

Because homozygous deletion of Plk1 ($Plk1^{-/-}$) results in embryonic lethal, but Plk1 heterozygotes ($Plk1^{+/-}$) and Plk2 null ($Plk2^{-/-}$) mice are viable (29, 49), we then attempted to breed $Plk2^{-/-}$ with $Plk1^{+/-}$ to determine whether we could genetically rescue the $Plk2^{-/-}$ phenotypes in mammary epithelial cells. Despite numerous matings, we were, however, unable to generate any offspring with the $Plk2^{-/-}$; $Plk1^{+/-}$ genotype (Supplementary Table S1). Further studies are required to determine the precise cause, but the synthetic lethality during embryonic development induced by the simultaneous loss of Plk2 and Plk1 suggested that there might be a genetic interaction between these two PLK family members.

Next, to examine whether PLK2 binds with PLK1, we performed a BiFC assay. A wild-type PLK2 (bait) was fused with the N-terminus of YFP and the PLK1 (prey) was fused with the C-terminus of YFP. If an interaction occurs between PLK2 and PLK1, the two YFP fragments will come together and form a fluorescent YFP protein that can be detected by a flow cytometer (Fig. 3A). Two previously identified substrates of PLK2, checkpoint kinase 1 (CHK1), and β-tubulin (TUBB) were used as positive preys (50, 51). RB transcriptional corepressor 1 (RB1) was included as a negative control prey, which was shown previously not to interact with Plk2 using an immunoprecipitation pull-down assay (50). Bait and prey constructs were stably transduced into cells and analyzed for YFP fluorescence by flow cytometry 48 hours posttransduction. As expected, strong interactions between PLK2 and the positive controls, CHK1 and TUBB, were detected, while the negative control, RB1, showed a very low percentage of YFP positivity (Fig. 3B). More importantly, a significant interaction between PLK2 and PLK1 was observed (Fig. 3B), thus indicating close physical proximity to one another in the cell.

A PLK2 (chr5:57785566-57791670)

Cancer Subset	In Peak?	Nearest Peak	#Genes in Peak	Q-value	Frequency of Deletion		
					Overall	Focal	High-level
all_cancers	No	chr5:58261529-59787458	2	4.96E-52	0.2515	0.0608	0.0328
Breast cancer	Yes	chr5:54834826-57786659	11	1.37E-4	0.2294	0.0493	0.0287
Lung adenocarcinoma	Yes	chr5:914233-180360469	1019	0.0048	0.2773	0.0532	0.0168
Acute myeloid leukemia	Yes	chr5:42547255-58652895	59	1.0	0.0155	0.0052	0.0
Ovarian serous carcinoma	No	chr5:58147456-59787458	2	9.55E-41	0.5506	0.2469	0.1439
Uterine and endometrial carcinoma	No	chr5:58261529-59787458	2	1.89E-10	0.1774	0.0605	0.0222
Head and neck squamous cell carcinoma	No	chr5:58261529-59787458	2	7.86E-4	0.371	0.0613	0.0226
Colorectal cancer	No	chr5:58261529-59787458	2	0.0207	0.1829	0.0274	0.0103
Lung squamous cell carcinoma	No	chr5:58261529-59787458	2	0.0635	0.686	0.0523	0.0523
Bladder cancer	No	chr5:58261529-59787458	2	0.118	0.4265	0.0809	0.0294
Glioblastoma multiforme	No	chr5:158528732-180360469	181	1.0	0.0293	0.0034	0.0052
Kidney clear cell carcinoma	No	No peak on chromosome	0	1.0	0.0161	0.0040	0.0020

Legend: Cancer-Promoter Significance	
$q \leq 0.25$	In a peak
$q \leq 0.25$	Not in a peak
$q > 0.25$	In a peak
$q > 0.25$	Not in a peak

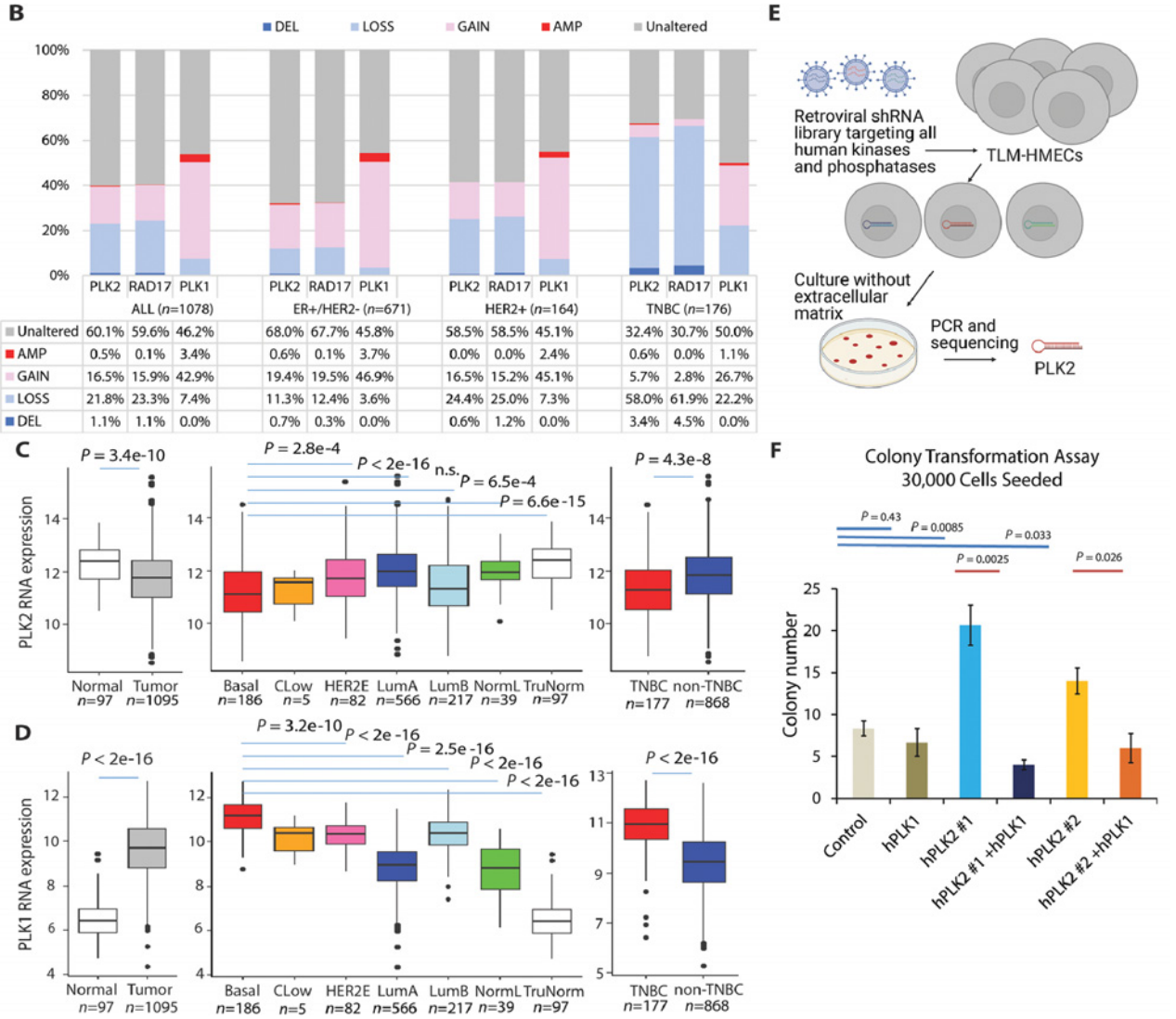

FIGURE 1 PLK2 is tumor suppressive and knockdown of PLK1 rescues PLK2 loss–induced transformation of HMECs. **A,** PLK2 is significantly deleted in 8 of 11 independent cancer types ($q \leq 0.25$) in the TCGA Pan-Cancer dataset (2013–08-16). Among these, PLK2 is located within a peak region of deletion in breast cancer and lung adenocarcinoma. **B,** PLK2, RAD17, and PLK1 CNAs in different breast cancer subtypes. Note that the loss of PLK2 and RAD17 is more dramatic in the TNBC subtype as compared with others. Amplification (Amp) >2.0, Gain >1.0, (*Continued on the following page.*)

(*Continued*) Deletion (Del) <2.0, Loss <1.0. PLK2 (**C**) and PLK1 (**D**) RNA expression vary significantly between normal breast tissue and breast tumor samples (left), intrinsic breast cancer subtypes (center), and triple-negative (TNBC) versus non-TNBC patients from the TCGA breast tumor dataset. *P* values shown from Student *t* test for two-class comparisons (normal vs. Tumor and TNBC vs. non-TNBC); *P* values between intrinsic subtypes are pairwise *t* tests with Bonferroni correction for multiple comparisons. **E,** Schematic of the unbiased RNAi-based forward genetic screen. TLM-HMECs need to be anchored to the extracellular matrix (ECM) to proliferate. Therefore, by applying a library of retroviral shRNAs targeting all human kinases and phosphatases to TLM-HMECs cultured in the absence of ECM, critical candidate genes involved in cell transformation could be discovered. The shRNA library was transduced into TLM-HMECs in duplicate. 530 anchorage-independent macroscopic colonies were quantitated from two independent screens. Colonies containing shRNAs were identified by PCR amplification and sequencing. **F,** Knockdown of PLK2 using two shRNAs increased the colony number for both, suggesting a tumor-suppressive role of PLK2 in HMECs. This induction was abolished by additional knockdown of PLK1. PLK1 shRNA alone did not show an effect on colony number formed in the colony transformation assay. 30,000 HMECs were seeded in the plates. Assays were performed in triplicate. Data are represented as mean ± SEM. Statistical significance was determined using unpaired two-tailed Student *t* test.

To confirm these findings at the single-cell level, we performed a complementary study using a proximity ligation assay (PLA) (Fig. 3C and D). In cells coexpressing both PLK1 and PLK2, we observed a strong positive PLA signal (red dots) as evidence for protein–protein interaction (Fig. 3C, image d). As shown by confocal imaging, both proteins were at close proximity to each other in cells at the G_2/M transition stage (presumably at the prometaphase stage), as evidenced by their rounded morphology and condensed nuclear DNA. Quantification revealed that 73% of 240 counted PLA-positive cells coexpressing PLK1 and PLK2 exhibited a rounded morphology, with the protein–protein interaction detected in the nucleus and/or perinuclear area (Fig. 3D). The percentage of those cells was increased to 93% after treatment with nocodazole (40 ng/mL, 16 hours), which induced cells to arrest in G_2/M phase (Supplementary Fig. S3B and S3C). No PLA signals were detected in nontransfected cells (Fig. 3C, image a), or in cells expressing only one of the proteins (Fig. 3C, images b and c). Additional negative controls were included for PLA performed in the absence of primary antibodies (Supplementary Fig. S3A, images a–d). These results indicated that the PLK2–PLK1 interaction is cell cycle dependent.

It is well established that the polo-box domain and kinase domain of PLK1 play significant roles in proper subcellular localization and cell cycle, as well as PLK1-dependent protein–protein interactions (52). Therefore, we tested PLK2-PBD [polo-box domain mutant (W503F, H629A, K631M) at the C-terminus] and PLK2-KD [kinase-dead mutant (K111R) at the N-terminus] mutants in the context of PLK1–PLK2 interaction using PLA. Contrary to our expectations, mutations at the polo-box domain of PLK2 did not disrupt PLK1–PLK2 interactions, and cells coexpressing PLK1 and PLK2-PBD mutant revealed a similar pattern for positive PLA signals as compared with those observed for cells co-transfected with PLK1 and wild-type PLK2 (Fig. 3C, image f). Most PLA signals were detected in the nucleus and perinuclear compartments, and 62% of 280 counted PLA-positive cells displayed rounded morphology with condensed DNA as a sign of prometaphase (Fig. 3D). Interestingly, in cells coexpressing PLK1 with PLK2-KD mutant, we observed positive PLA signals predominantly in the cytoplasm and 69% of 300 counted cells had a flat and elongated morphology with noncondensed DNA, clearly showing that interaction between the two proteins mostly occurs during the interphase but not the mitosis (Fig. 3C, image h, and D). In addition, the percentage of such cells did not significantly change following nocodazole treatment (Supplementary Fig. S3B and S3C). These data suggest that the kinase domain of PLK2 most likely plays an important role in maintaining proper protein–protein interactions between PLK1 and PLK2 during the prometaphase stage of a cell cycle. No PLA signals were detected in cells expressing PLK2-PBD or PLK2-KD mutants alone (Fig. 3C, images e and g), or when PLA was performed in the absence of primary antibodies (Supplementary Fig. S3A, images e–h).

Low PLK2 May Serve as a Biomarker to Predict Response to the PLK1 Inhibitor

The previous combination of biochemical, genetic, and bioinformatic studies suggests that inhibiting PLK1 in a setting with low PLK2 expression, such as TNBC, may provide a targeted approach for a disease in which chemotherapy is still the only systematic treatment (53). Therefore, we tested the effects of a PLK1 inhibitor both as a single agent and in combination with chemotherapy in both novel $p53^{-/-}$ GEM and PDX preclinical models with low versus high PLK2 expression.

To develop appropriate preclinical models, we used $p53^{-/-}$ mice as a sensitized background to generate $Plk2^{-/-}$; $p53^{-/-}$ murine mammary tumors in a manner similar to that used previously to develop a bank of transplantable $p53^{-/-}$ tumors in Balb/c mice (ref. 54; Supplementary Fig. S4), the latter of which have been extensively characterized in our laboratories (55). Following transplantation of the $Plk2^{-/-}$; $p53^{-/-}$ MECs into the cleared fat pad of wild-type Balb/c recipients, palpable tumors were observed following an 8-month to more than a one-year latency period, similar to that observed previously for $p53^{-/-}$ MECs. RNA-seq analysis showed that they can be classified into three distinct molecular TNBC subtypes designated as luminal-like, basal-like, and claudin-low similar to $p53^{-/-}$ mammary tumors (Supplementary Fig. S5). Evidence for these classifications comes through the examination of overall expression patterns (Supplementary Fig. S5) as well as known key subtype defining genes (Supplementary Fig. S6).

To determine proper controls for our mammary tumors, we conducted a hierarchical clustering analysis on RNA-seq datasets of 192 murine mammary tumor samples, and identified the closest $p53^{-/-}$ tumors for each $Plk2^{-/-}$; $p53^{-/-}$ TNBC subtype (Supplementary Table S2; Supplementary Fig. S5). We next performed mammary fat pad transplantation for all the matched genotypes/subtypes of tumors and tested four treatment conditions: vehicle control, carboplatin alone, PLK1 inhibitor volasertib alone, as well as a combination of carboplatin and volasertib. Pilot experiments using volasertib (50 mg/kg/week, a tolerated dose using colon carcinoma PDX models; ref. 56) plus carboplatin showed a strong therapeutic effect in $Plk2^{-/-}$; $p53^{-/-}$ claudin-low tumors, but not $p53^{-/-}$ claudin-low tumors (Supplementary Fig. S7A and S7B). However, this dosage is also toxic as the mice had body weight loss and some mice in volasertib treatment groups, and carboplatin plus volasertib groups, eventually died (Supplementary Fig. S7C and S7D). We then reduced the dose to

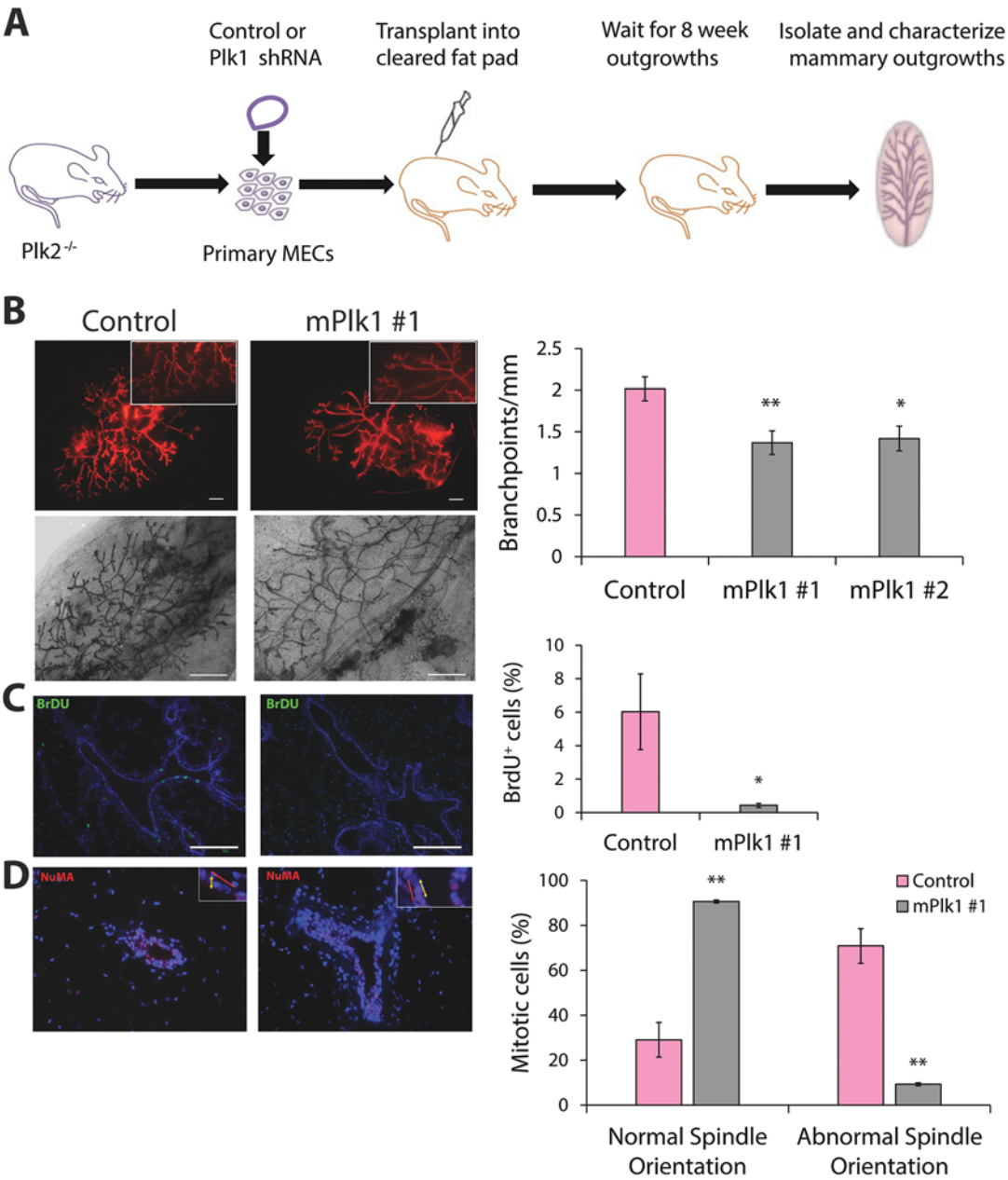

FIGURE 2 Knockdown of Plk1 rescues the Plk2$^{-/-}$ mammary gland phenotypes. **A,** Schematic representation of the experimental procedure used to determine the effect of Plk1 shRNA knockdown on Plk2$^{-/-}$ MECs. Briefly, MECs were isolated from Plk2$^{-/-}$ mice, transduced with lentiviral vectors containing control or mPlk1 shRNAs, and then injected into wild-type SCID/Beige mice with cleared mammary fat pad. After 8 weeks, we harvested and characterized the outgrowths. **B,** Whole-mount analyses of mammary glands transduced with control or Plk1 shRNAs showed a decrease in branching upon depletion of Plk1. $n = 10$ mice for Control group, $n = 3$ mice for mPlk1 #1 group, $n = 7$ mice for mPlk1 #2 group. Td-tomato red expression in the transduced cells is shown in the whole-mounts (top left). Bottom left, carmine alum staining. Representative pictures of mPlk1 #1 shRNA group were shown. The right panel shows the quantitation of branch points per millimeter. **C,** Immunofluorescence for BrdU (green) incorporation and DAPI (blue) on paraffin-embedded sections of mammary glands demonstrated that knockdown of Plk1 abolished the hyperproliferation phenotype of Plk2$^{-/-}$ MECs (ref. 31; left panel). $n = 3$ mice per group. Right, the quantitation of BrdU-positive MECs. **D,** Disruption of mitotic spindle orientation in Plk2$^{-/-}$ MECs was rescued by knockdown of Plk1. Normal spindle orientation was defined as the angle between the basement membrane and the plane of the mitotic spindle being 0–10°, while abnormal being 10–90°. Mice were treated with estrogen and progesterone for two days to induce epithelial cell proliferation. $n = 3$ mice per group. Nuclear mitotic apparatus protein 1 (NuMA; red) was used to stain the mitotic spindle. DAPI (blue) counterstained the nucleus. The red line indicates the proper plane of cell division and the yellow arrows denote the actual plane of division. Right, the quantitation of normal and abnormal spindle orientation. Data are represented as mean ± SEM. Statistical significance was determined by unpaired two-tailed Student *t* test compared with the control group. *, $P < 0.05$; **, $P < 0.01$.

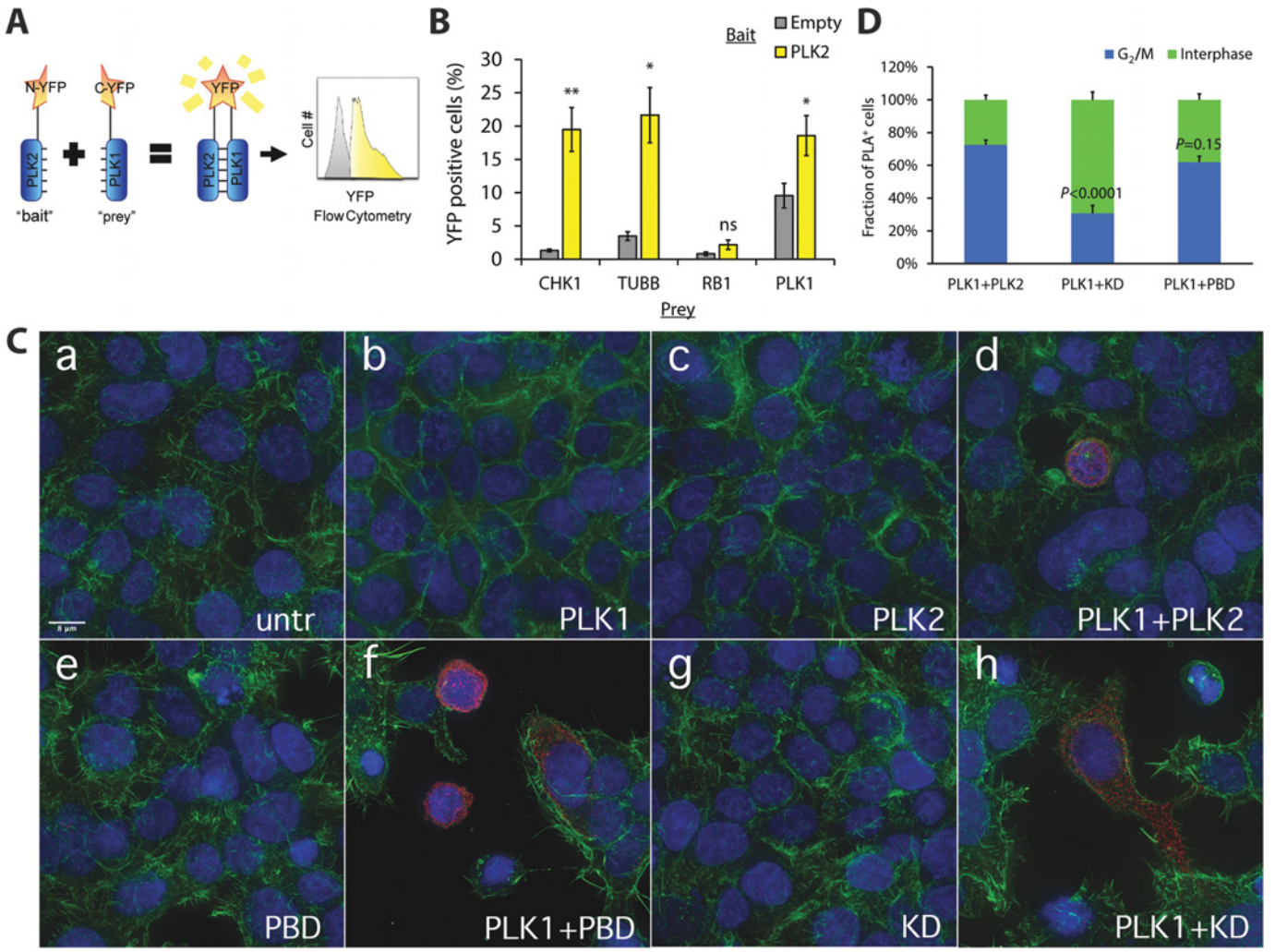

FIGURE 3 PLK2 directly interacts with PLK1. **A,** Diagram of BiFC assay. The prey fused with the C-terminus of YFP is added to the bait fused with the N-terminus of YFP. If an interaction occurs between the prey and the bait, the two YFP fragments will come together and form a fluorescent YFP that can be analyzed by flow cytometry. **B,** PLK2 directly interacted with PLK1 as well as CHK1 and TUBB. As predicted, no interaction was observed between PLK2 and RB1. Assays were repeated five times in triplicate using HEK293T cells. Statistical significance was determined by unpaired two tailed student's t-test. Ns, not significant; *, $P < 0.05$; **, $P < 0.01$. **C,** Proximity ligation assay in HEK293T cells co-expressing PLK1 with PLK2-wild-type, PLK2-PBD, or PLK2-KD mutants. Red, PLA signals. Blue, DAPI nuclei staining. Green, ß-actin staining. Representative images with positive PLA signals for the interaction of PLK1 with PLK2 (image d), PLK1 with PLK2-PBD (polo-box domain mutant) (image f), and PLK1 with PLK2-KD (kinase-dead mutant) (image h) are shown. Negative controls: nontransfected cells (image a); cells expressing only one protein: PLK1 (image b), PLK2 (image c), PLK2-PBD (image e), or PLK2-KD (image g). Note that the PLA signals of PLK1+PLK2 and PLK1+PBD are located at the nucleus and/or perinuclear area of round G_2/M cells while the PLA signals of PLK1+KD are located in the cytoplasm of flat and elongated interphase cells. Scale bar is representatively depicted in image a and equals 8 μm. **D,** Quantitative analysis of PLA signals in cells co-expressing PLK1 with wild-type PLK2, PLK2-PBD, and PLK2-KD mutants using microscopy images. PLA-positive cells were divided into two groups: cells that have rounded morphology with condensed nuclear DNA were considered mitotic (G_2/M), while cells with flat and elongated morphology and noncondensed nuclear DNA were considered to be in interphase of the cell cycle. PLA-positive cells (200 to 300) were counted per group. Data are represented as mean ± SEM. Statistical significance was determined by one-way ANOVA followed by Tukey test for multiple comparisons.

25 mg/kg/week, which was well tolerated by all GEM models (Supplementary Fig. S8). We found that Plk2$^{-/-}$; p53$^{-/-}$ claudin-low, basal-like and luminal-like tumors showed a markedly better response to the combinational treatment as compared with their paired p53$^{-/-}$ tumors with wild-type Plk2 expression (Fig. 4). Statistical analysis comparing the $\log_2$ fold change in different tumor types when the control treatment group reached approximately 1,500 mm^3 confirmed the significant differences among these models as a function of Plk2 expression (Fig. 4C, F and I). Collectively, these data suggested that PLK1 inhibition in combination with chemotherapy is more effective in treating TNBC that has low PLK2 expression.

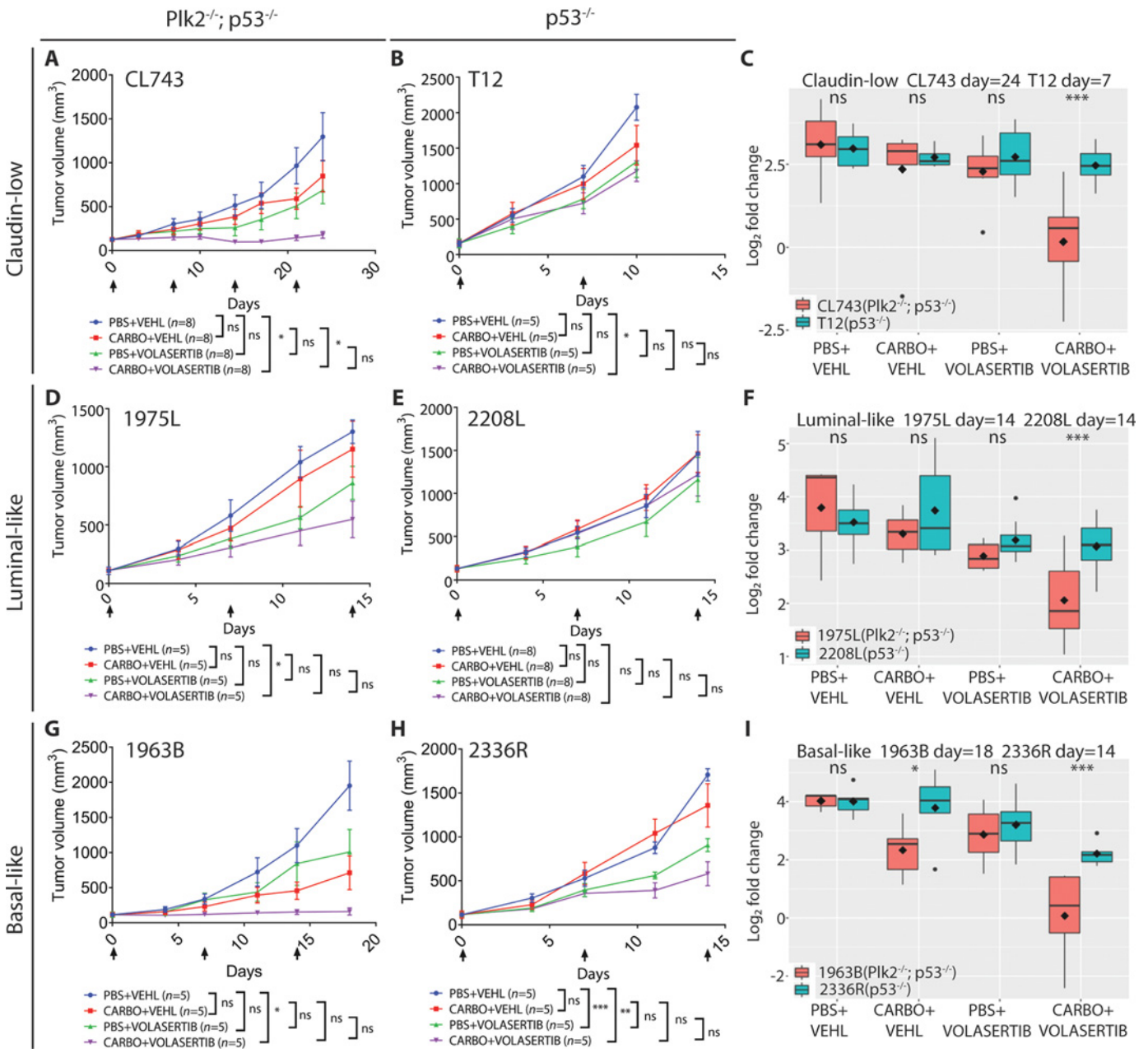

FIGURE 4 Plk2$^{-/-}$; p53$^{-/-}$ mammary tumors respond better to the combinational treatment of carboplatin plus the Plk1 inhibitor volasertib than their subtype-matched Plk2$^{+/+}$; p53$^{-/-}$ control tumors. Tumor growth curves of claudin-low subtypes CL743 and T12 (**A** and **B**), luminal-like subtypes 1975 L and 2208 L (**D** and **E**), basal-like subtypes 1963B and 2336R (**G** and **H**). Tumor size was measured using a digital caliper twice a week until control groups reached ~1,500 mm^3. Two-way ANOVA followed by Tukey test for multiple comparisons was used to analyze the growth curves of **A**, **B**, **D**, **E**, **G**, and **H**. Statistical comparison of the experimental endpoint was shown. **C, F,** and **I,** Comparison of $\log_2$ fold change of tumor size between same treatment groups of Plk2$^{-/-}$; p53$^{-/-}$ tumors, and p53$^{-/-}$ tumors. Data are represented as mean ± SEM. Linear hypothesis test from the R package was used to compare the same treatment groups between different tumor models of **C**, **F**, **I**. Arrows indicate when the mice were treated. VEHL, vehicle; CARBO, carboplatin; ns, not significant. *, $P < 0.05$; **, $P < 0.01$; ***$P < 0.001$.

Because many TNBC tumors are polyploid, and basal-like subtypes are often 3N (57), PLK2 expression is markedly reduced but rarely completely deleted. While the Plk2$^{-/-}$; p53$^{-/-}$ GEMs provided models for complete Plk2 deletion, we extended our studies to several TNBC PDX models with high or low PLK2 expression to evaluate the relevance between the response to PLK1 inhibition plus chemotherapy and chromosome 5q loss/PLK2 loss (Supplementary Fig. S9). We identified six PDX models from the Baylor College of Medicine breast cancer PDX collection according to their PLK2 mRNA expression and known response to carboplatin from an ongoing preclinical trial, and tested the efficacy of volasertib in combination with carboplatin. We divided the six PDX models

into three groups based on their response to carboplatin: complete responders, partial responders, and nonresponders. In both complete carboplatin responders and partial responders, PDX models with lower PLK2 expression had a better response to volasertib, which induced tumor cytostasis (BCM-0002 vs. BCM-7482, BCM-2665 vs. BCM-15003; Fig. 5A, C, E, G, and I; Supplementary Fig. S10 and S11). In contrast, tumor models with higher PLK2 expression continued to grow under volasertib administration, although at a slower rate compared with their controls (Fig. 5B, D, F, H, and I; Supplementary Fig. S10 and S11). Comparison of PLK2-low PDX lines to PLK2-high PDX lines when $\log_2$ fold change of control groups reached 2.5 suggested that volasertib has a better tumor growth–inhibitory effect in PLK2-low PDX lines (Fig. 5E–I). However, in nonresponders, although volasertib slowed tumor growth of the model with lower PLK2 expression (BCM-4664), there was one exception where it induced a complete response in the PDX model with higher PLK2 expression (HCI-027; Supplementary Fig. S10).

To understand the relationship between PLK2 loss and carboplatin treatment in predicting response to PLK1 inhibitors, we performed data mining on current clinical trials. Unfortunately, no clinical trial data are available using volasertib in combination with chemotherapy in patients with TNBC. Nonetheless, by analyzing the recently published BrighTNess phase III neoadjuvant clinical trial in which carboplatin was added to standard neoadjuvant chemotherapy for patients with TNBC (58), we observed a lower RNA expression level of PLK2, a higher level of PLK1, and a negative correlation between PLK1 and PLK2 expression in those patients whose tumors achieved a pathologic complete response as compared with those with residual disease (Supplementary Fig. S12). This provides additional support for the potential clinical relevance of PLK2 loss and carboplatin response.

To further determine the role of PLK2 in predicting the response to PLK1 inhibitor, we established two doxycycline-inducible isogenic models. First, we generated a mouse tumor cell line taking advantage of the residual neomycin cassette from the 1963B tumors ($Plk2^{-/-}$; $p53^{-/-}$ basal-like TNBC). Second, we examined the CNVs of the breast cancer cell lines from the Broad Institute. Surprisingly, almost none of the existing established human breast cancer cell lines exhibited a loss of PLK2 (see Discussion). Only the BT20 cell line was identified to exhibit partial PLK2 and MAP3K1 (another chromosome 5q marker) loss (Supplementary Fig. S13). Interestingly, BT20 xenografts exhibited an extremely long latency in NSG mice (Supplementary Fig. S14). We then infected both cell lines with the doxycycline-inducible vector pCW57.1 containing PLK2 and implanted the mouse 1963B-iPLK2 and human BT20-iPLK2 cells into the fourth mammary fat pad of Balb/c and NSG mice, respectively. Restored PLK2 expression by doxycycline was validated by qPCR and Western blot analysis (Fig. 6A and B; Supplementary Fig. S14A and S14B). Volasertib treatment significantly reduced the tumor growth rate in both 1963B-iPLK2 and BT20-iPLK2 tumors in the absence of doxycycline induction (Fig. 6C; Supplementary Fig. S14C). Strikingly, doxycycline induction of PLK2 expression resulted in decreased volasertib inhibition of tumor growth at the experimental endpoints in both models (Fig. 6C; Supplementary Fig. S14C and S15). Comparison of $\log_2$ fold change of tumor volume starting from the drug treatment to the experimental endpoint confirmed the reduced effect of volasertib in doxycycline-treated 1963B-iPLK2 tumors (Fig. 6D). Taken together, these studies provide support in isogenic models that PLK2 loss may serve as a potential biomarker to identify patients with TNBC likely to be responsive to PLK1 inhibition.

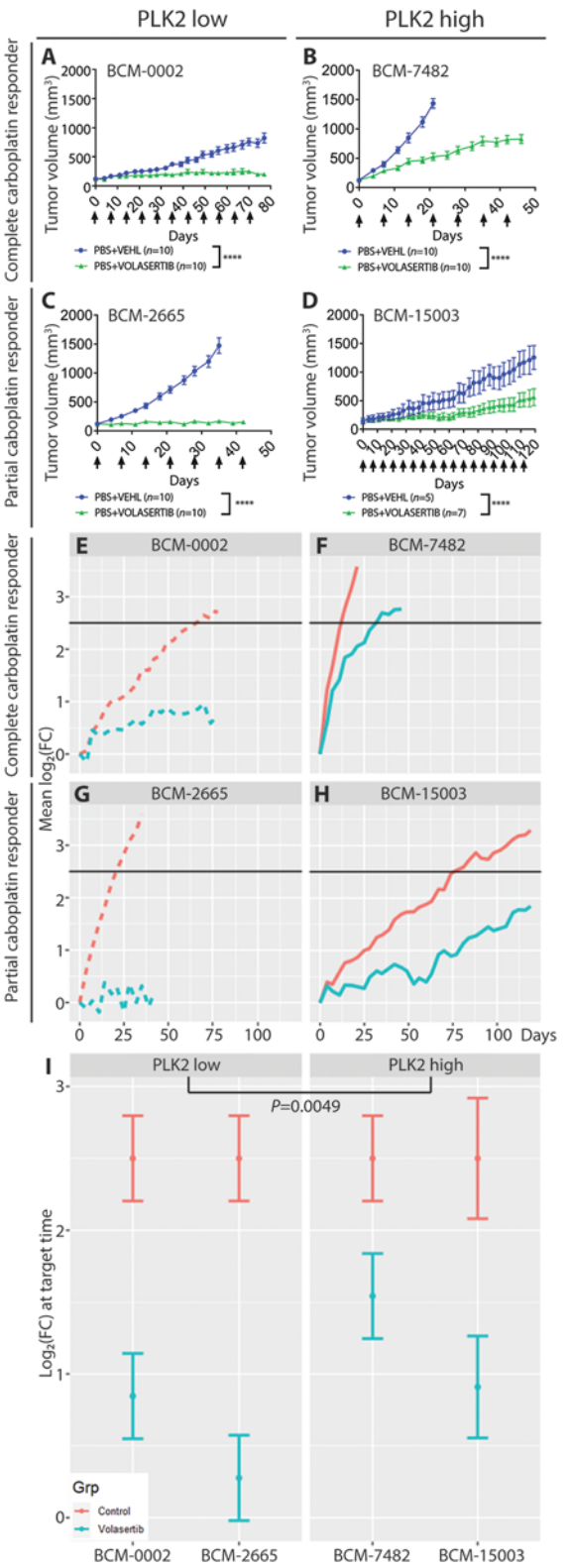

FIGURE 5 TNBC PDX with low *PLK2* expression had a better response to volasertib treatment than TNBC PDX with high *PLK2* expression if they showed response to carboplatin treatment. (**A** and **B**) BCM-0002 and BCM-7482 were complete (*Continued on the following page.*)

(*Continued*) responders to carboplatin treatment. (**C** and **D**) BCM-2665 and BCM-15003 showed partial response to carboplatin treatment. Note that volasertib treatment induced tumor cytostasis in BCM-0002 and BCM-2665. Tumor size was measured using a digital caliper twice a week. Data are represented as mean ± SEM. Two-way ANOVA followed by Tukey test for multiple comparisons was used to analyze the growth curves for each model. Statistical comparison at the endpoint of control group was shown. VEHL, vehicle; ****, $P < 0.0001$. **E–H**, Mean $\log_2$ tumor size fold change (FC) from baseline for each PDX line and treatment group. The target log2(FC) (2.5 in the control group, black line) was used for statistical analysis of panel I. **I,** A linear contrast was constructed to test whether the average difference in $\log_2$(FC) of tumor size increment between control and volasertib in the PLK2-low PDX lines is the same as the PLK2-high PDX lines.

Discussion

Several chemotherapy drugs, either singly or in combination, including doxorubicin, cyclophosphamide, paclitaxel, and carboplatin, are still the standard-of-care therapy for many types of cancer, including breast cancer (59). However, these drugs have substantial side effects and limitations such as toxicity, immunosuppression, and drug resistance (60). In recent years, there has been a focus on developing new selective antimitotic drugs to help overcome some of these issues. PLK1 is a popular target as it regulates multiple essential steps of mitosis (61). Overexpression of PLK1 has been found in multiple types of solid tumors as well as in leukemia, and correlated with poor prognosis and survival (61). Several PLK1 inhibitors are currently in clinical development, including volasertib (62). In this study, we found that PLK2-loss may provide a biomarker to guide PLK1 inhibitor patient selection, and furthermore, that it may be effective at a lower dose with reduced toxicity.

Unlike the well-established oncogenic function of PLK1, the role of PLK2 in human cancers remains unclear. PLK2 has been reported to be tumor suppressive in B-cell neoplasia, laryngeal carcinoma, cervical cancer cell lines, and patient samples by promoting apoptosis and inhibiting cell proliferation (34, 63, 64). On the other hand, PLK2 expression was also correlated with improved cell survival using knockdown techniques in head and neck cancer and non–small cell lung cancer cell lines (50, 65). Contradictory effects of PLK2 in colorectal cancer also have been reported. One study showed that PLK2 promoted colorectal cancer growth and inhibited apoptosis by targeting Fbxw7/Cyclin E (66). In contrast, another study suggested that PLK2 was a tumor suppressor and its loss was more common in colorectal carcinoma than adenomas (67). Therefore, the role of PLK2 appears to be tumor type- and/or stage-dependent. In this study, using a genetic shRNA screen, we observed that loss of PLK2 promoted colony formation of human mammary epithelial cells. Bioinformatic analysis of several human breast tumor datasets also indicated that PLK2 (chromosome 5q11.2) is located within a peak region of frequent deletion in breast cancer, consistent with previously published studies (47); moreover, the same chromosomal region is frequently deleted in several other cancers (9, 10). Furthermore, PLK2 mRNA expression is significantly lower in breast cancer as reported in the TCGA dataset. Therefore, it is conceivable that PLK2 is tumor suppressive in breast cancer, specifically that chromosomal loss of PLK2 is highly enriched within the basal-like/triple-negative subtypes of breast cancer. In agreement with this finding, we found that PLK2 mRNA expression in TNBC is the lowest as compared with other breast cancer subtypes.

Despite the fact Plk1 heterozygotes ($Plk1^{+/-}$) and Plk2-null ($Plk2^{-/-}$) mice are viable (29, 49), we observed a synthetic lethal phenotype of $Plk2^{-/-}$; $Plk1^{+/-}$ offspring, suggesting a potential genetic interaction/compensation between PLK2 and PLK1. Therefore, we tested whether PLK2 can interact with PLK1 using two independent methods: BiFC and PLA. Both methods indicated an interaction between PLK2 and PLK1. Two PLK2 mutants analyzed using the PLA revealed that the kinase domain, but not the polo-box domains, of PLK2 is responsible for their interaction at prometaphase. While these studies have helped shed light on interactions with target substrates and the importance of proper subcellular localization and cell cycle, the precise mechanism of how PLK2 might regulate PLK1 during prometaphase is still unclear. It has been reported that PLK2 can phosphorylate Ser-137 of PLK1 to promote human colon cancer cell survival in cells with mitochondrial dysfunction (68). Given that PLK2–PLK1 interaction at prometaphase was mediated by PLK2 kinase domain, it is tantalizing to speculate that PLK2 may phosphorylate PLK1 to regulate cell-cycle progression in normal mammalian epithelial cells and that loss of PLK2 may change PLK1 subcellular location and cell cycle–dependent activity, thereby leading to a mitotic catastrophe and promoting tumor growth. However, phosphorylation of Thr-210 in the T-loop of the PLK1 kinase domain by Bora/Aurora-A–dependent phosphorylation is thought to be required for mitotic entry (69). Thus, the underlying mechanism of how PLK2 regulates PLK1 warrants further investigation.

Despite the rapid progress in the development of PLK1 inhibitors, there is a lack of biomarkers that can predict a patient's response to this treatment. A recent study showed that targeting PLK1 using volasertib induced synthetic lethality in BRCA1-deficient cells (70), thus suggesting BRCA1 may serve as a biomarker for the response to PLK1 inhibition treatment. Our findings that PLK1 might mediate PLK2 function both *in vitro* and *in vivo* encouraged us to investigate the implication of PLK2 loss in the context of PLK1 inhibitor treatment.

DePinho and colleagues found that ENO1 was often deleted in glioblastomas and rendered glioma cells more sensitive to the inhibition of ENO2, herein proposed collateral damage caused by passenger deletions of redundant essential genes as a novel therapeutic strategy (71). In line with this concept, we found that PLK2-low TNBC tumors were more sensitive to volasertib plus carboplatin in our rapidly growing GEM models across all of the three molecular subtypes of TNBC studied. This was also observed in several pairs of PLK2-high and -low PDX models with much more complex genetics, with one notable exception (HCI-027) where a marked response to volasertib was observed in the absence of low Plk2 expression; this may reflect the high level of PLK1 protein expression in this model (Supplementary Fig. S9C), but further studies will be required to understand the mechanisms responsible. Thus, as expected from the complex genetics of TNBC, decreased PLK2 expression alone may not always suffice to predict response to PLK1 inhibitors; however, low PLK2 expression does appear to at least highly enrich for PLK1 inhibitor responsiveness. It is also possibly that PLK2 is one of the many target genes of deletion in the chromosome 5q region that contribute to the PLK1 inhibition sensitivity together.

Volasertib worked better in PLK2-low/deleted models when treated together with carboplatin. Carboplatin is known to block DNA replication and transcription and induce cell death (72). However, the molecular mechanisms underlying the resistance and sensitivity of tumors to carboplatin are still under investigation. Given the important role of the PLK family in cell cycle and proliferation, loss of PLK2 in tumors may render them more sensitive to carboplatin plus volasertib through some shared mechanisms related to

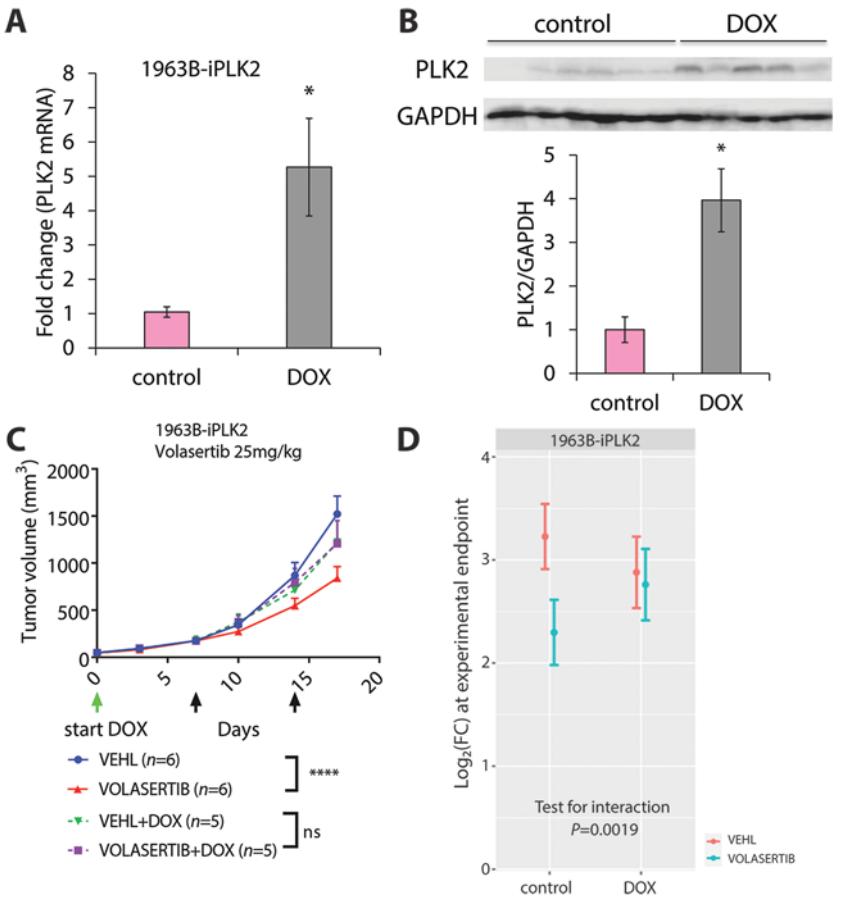

FIGURE 6 Doxycycline-induced PLK2 expression abolished the therapeutic effect of volasertib in mouse Plk2$^{-/-}$; p53$^{-/-}$ 1963B basal-like breast tumors. **A,** qPCR analysis showed that PLK2 mRNA expression was induced by doxycycline water (DOX) in the mouse 1963B-iPLK2 tumors. $n = 6$ for 1963B-iPLK2 control group. $n = 5$ for 1963B-iPLK2 doxycycline group. Data are represented as mean ± SEM. Statistical significance was determined by unpaired two-tailed Student t test. *, $P < 0.05$. **B,** Western blot analysis and quantification showed that PLK2 protein expression was induced by doxycycline in the mouse 1963B-iPLK2 tumors. $n = 6$ for 1963B-iPLK2 control group. $n = 5$ for 1963B-iPLK2 doxycycline group. Data are represented as mean ± SEM. Statistical significance was determined by unpaired two-tailed Student t test. *, $P < 0.05$. **C,** Tumor growth curves of mouse tumors under vehicle and volasertib treatment with or without doxycycline. Note that volasertib treatment significantly reduced tumor growth for non-doxycycline–treated tumors but not doxycycline -treated tumors at the experimental endpoints. Tumor size was measured using a digital caliper twice a week. Data are represented as mean ± SEM. Two-way ANOVA followed by Tukey test for multiple comparisons was used to analyze the growth curves. Statistical comparison of the experimental endpoint was shown. Green arrow indicates when doxycycline treatment began. Black arrows indicate when the mice were treated with drugs. VEHL, vehicle; ns, not significant; ****, $P < 0.0001$. **D,** Two-way ANOVA analysis of $\log_2$ fold change (FC) of tumor volume starting from drug treatment to the end of experiment confirmed the reduced tumor-inhibitory effect of volasertib in doxycycline-treated 1963B-iPLK2 tumors.

cell proliferation and cell death. Analysis of BrighTNess clinical trial, which added carboplatin to standard neoadjuvant chemotherapy for patients with TNBC, supports the potential translational relevance of PLK2 loss and carboplatin response. In agreement with this analysis, our study of restoring PLK2 in the mouse Plk2$^{-/-}$; p53$^{-/-}$ 1963B-iPLK2 basal-like tumors showed that carboplatin response was blocked by doxycycline-induced PLK2 expression (Supplementary Fig. S15). Another possibility may be that carboplatin could induce DNA damage and our previous study showed that knockdown of DNA repair gene *RAD17* in immortalized HMECs increased sensitivity to carboplatin (47, 73). This may help to explain the need of carboplatin response to predict the response to PLK1 inhibition in our PDX models in which the loss of chromosome 5q typically includes both PLK2 and RAD17. Similarly, the increased sensitivity to volasertib plus carboplatin in our GEM models may not only be due to Plk2 loss but also the loss of p53, which is critical to DNA repair. Nonetheless, further studies are needed to uncover the underlying mechanisms.

The synthetic lethality observed between Plk1$^{+/-}$ and Plk2$^{-/-}$ mice indicates that PLK2 loss may sensitize tumors to lower doses of PLK1 inhibitors. In this study, treatment with carboplatin and volasertib was performed at approximately 50% of the reported clinically relevant doses of each as a single agent, without any apparent toxicity as revealed by weight loss or mortality. These results suggest that it may be possible to reduce the toxicity of these individual agents by dose deescalation studies done in combination, although this issue is beyond the scope of this study or the statistical power of the mouse studies

performed. Also, as the combinational drug treatment regimens are evolving (74), it will be interesting to examine whether carboplatin and volasertib can be administrated in a sequential treatment strategy or an alternating dosing schedule.

To identify a human breast cancer cell line with PLK2 loss for our study, we screened the Broad Institute breast cancer cell line database and surprisingly found that the deletion of PLK2 and other nearby chromosome 5q genes was rarely observed in breast cancer cell lines in contrast to established PDX models and patient TCGA datasets (Fig. 1; Supplementary Figs. S1 and S13). This suggests that loss of PLK2/ chromosome 5q was selected against under *in vitro* cell culture conditions. Furthermore, PDX models are a better representation of the tumor status in patients. Nevertheless, we identified BT20 as a PLK2-low model and generated a doxycycline-inducible PLK2 system. In previous studies, both when implanted subcutaneously or orthotopically in the mammary fat pad, BT20 cells exhibit a delayed growth response and have recently been shown to fail to metastasize following intracardiac injection (75–78). Notwithstanding the delayed growth kinetics, together with the doxycycline-inducible PLK2 mouse tumor model, we demonstrated that a higher level of PLK2 expression was able to impair the therapeutic effect of volasertib at the experimental endpoint. Thus, these results obtained in both mouse and human isogenic models help support the role of PLK2 as a biomarker for predicting response to the PLK1 inhibitor.

Volasertib is an ATP-competitive compound for the PLK1 kinase domain and we found that the kinase domain of PLK2, but not the PBD, played an essential role in PLK2–PLK1 interaction. It will be interesting to examine whether TNBC patients with low PLK2 expression can benefit from the treatment with PBD-binding antagonists, another class of PLK1 inhibition drugs. Because PBD is unique for the PLK family and required for their functions, compounds specially targeting PBD represent an ideal group of PLK inhibitors. Poloppin, a recently developed PBD inhibitor, was shown to effectively target KRAS-expressing colorectal cancer xenografts (79). Therefore, comparing treatment study using poloppin to volasertib may yield more information about PLK2–PLK1 interactions and benefit patients with breast cancer with a more precise treatment.

Beroukhim and colleagues reported previously that chromosome 5q loss containing PLK2 was one of the top 20 most significant peak deletion regions detected across 26 types of human cancers (9). Taylor and colleagues (10) and our unpublished studies (Siegel, Perou, and colleagues, manuscript in preparation), have also revealed that chromosome 5q loss often occurs in lung squamous cell carcinoma, ovarian cancer, as well as TNBC. Therefore, the utility of PLK2 as a biomarker may have a broader application and provide a therapeutic window for the use of PLK1 inhibitors in multiple types of cancers.

Authors' Disclosures

D. Acosta reports grants from National Institute of General Medical Sciences (NIGMS) during the conduct of the study. L.E. Dobrolecki reports personal fees from StemMed, Ltd. outside the submitted work. M.T. Lewis reports grants from CPRIT (grant number RP170691); and grants from NCI (grant number U54 CA224076) during the conduct of the study; other from StemMed Ltd (limited partner) and other from Tvardi Therapeutics Inc. (equity holder) outside the submitted work; and some patient-derived xenograft models are licensed to StemMed Ltd. for which Dr. Lewis receives royalties. C.M. Perou reports personal fees from Bioclassifier LLC (equity stock holder and royalties) outside the submitted work; in addition, C.M. Perou has a patent for U.S. Patent No. 12,995,459 issued, licensed, and with royalties paid from Bioclassifier. No other disclosures were reported.

Authors' Contributions

Y. Gao: Conceptualization, data curation, formal analysis, funding acquisition, validation, investigation, visualization, methodology, writing-original draft, project administration, writing-review and editing. **E.B. Kabotyanski:** Data curation, formal analysis, validation, investigation, visualization, methodology, writing-review and editing. **J.H. Shepherd:** Data curation, formal analysis, investigation. **E. Villegas:** Data curation, investigation, visualization, methodology. **D. Acosta:** Investigation, methodology. **C. Hamor:** Investigation. **T. Sun:** Investigation, methodology. **C. Montmeyor-Garcia:** Investigation, methodology. **X. He:** Project administration. **L.E. Dobrolecki:** Resources, project administration. **T.F. Westbrook:** Conceptualization, project administration, writing-review and editing. **M.T. Lewis:** Funding acquisition, project administration, writing-review and editing. **S.G. Hilsenback:** Formal analysis, funding acquisition, methodology. **X.H.-F. Zhang:** Formal analysis, funding acquisition, methodology, project administration, writing-review and editing. **C.M. Perou:** Conceptualization, funding acquisition, project administration, writing-review and editing. **J.M. Rosen:** Conceptualization, resources, supervision, funding acquisition, project administration, writing-review and editing.

Acknowledgments

This study was funded by the following grants: Susan G. Komen (SAC110031, to J.M. Rosen; SAC160074, to C.M. Perou), NCI Breast SPORE program (P50-CA58223), and the NIH (R01-CA148761, to J.M. Rosen and C.M. Perou). Y. Gao received training support from the Translational Breast Cancer Research Training Program (NIH T32 CA203690, PI: Suzanne Fuqua). Imaging for this project was supported by the Integrated Microscopy Core at Baylor College of Medicine with funding from NIH (DK56338 and CA125123), CPRIT (RP150578, RP170719), the Dan L. Duncan Comprehensive Cancer Center, and the John S. Dunn Gulf Coast Consortium for Chemical Genomics. This project was also supported by the Cytometry and Cell Sorting Core at Baylor College of Medicine with funding from the CPRIT Core Facility Support Award (CPRIT-RP180672), the NIH (P30 CA125123 and S10 RR024574) and the expert assistance of Amanda White and Joel M. Sederstrom. PDX study was supported by Patient-Derived Xenograft and Advanced In Vivo Models Core at Baylor College of Medicine (Michael T. Lewis, PhD, Academic Director, Lacey E. Dobrolecki, M.S., Technical Director. Grants supporting the core: CPRIT Core Facility Award (RP170691) and P30 Cancer Center Support Grant (NCI-CA125123)). Statistical analysis was supported by Biostatistics and Informatics Shared Resource Core (Susan G. Hilsenbeck, PhD, Director. Grants supporting: CCSG P30CA125123 and SPORE P50CA186784).The authors also thank Dr. Meenakshi Anurag for her help with the BrighTNess clinical trial analysis and Dr. Chad A. Shaw for the initial bioinformatic analyses of TCGA data; Ramakrishnan Rajaram Srinivasan for analyzing PLK2 and PLK1 mRNA expression of PDX models; Hannah Johnson for assisting with imaging; Shirley Small for her help with animal experiments; Dr. Kristen L. Karlin for providing the human PLK1 shRNA; Dr. Yating Cheng for her help with cloning; Dr. Xi Chen for sharing the equipment; and Dr. Alana Welm, Dr. Helen Piwnica-Worms, and Dr. Gloria Echeverria for their helpful discussion.

Received October 28, 2021; revised November 29, 2021; accepted December 09, 2021; published first December 27, 2021.

References

1. Siegel RL, Miller KD, Fuchs HE, Jemal A. Cancer Statistics, 2021. CA Cancer J Clin 2021;71: 7-33.
2. Schnitt SJ. Classification and prognosis of invasive breast cancer: from morphology to molecular taxonomy. Mod Pathol 2010;23: S60-4.
3. Cancer Genome Atlas Network. Comprehensive molecular portraits of human breast tumours. Nature 2012;490: 61-70.
4. Fisher B, Costantino J, Redmond C, Poisson R, Bowman D, Couture J, et al. A randomized clinical trial evaluating tamoxifen in the treatment of patients with node-negative breast cancer who have estrogen-receptor-positive tumors. N Engl J Med 1989;320: 479-84.
5. Fisher B, Jeong JH, Bryant J, Anderson S, Dignam J, Fisher ER, et al. Treatment of lymph-node-negative, oestrogen-receptor-positive breast cancer: long-term findings from National Surgical Adjuvant Breast and Bowel Project randomised clinical trials. Lancet 2004;364: 858-68.
6. Vogel CL, Cobleigh MA, Tripathy D, Gutheil JC, Harris LN, Fehrenbacher L, et al. Efficacy and safety of trastuzumab as a single agent in first-line treatment of HER2-overexpressing metastatic breast cancer. J Clin Oncol 2002;20: 719-26.
7. Ménard S, Pupa SM, Campiglio M, Tagliabue E. Biologic and therapeutic role of HER2 in cancer. Oncogene 2003;22: 6570-8.
8. Paik S, Shak S, Tang G, Kim C, Baker J, Cronin M, et al. A multigene assay to predict recurrence of tamoxifen-treated, node-negative breast cancer. N Engl J Med 2004;351: 2817-26.
9. Beroukhim R, Mermel CH, Porter D, Wei G, Raychaudhuri S, Donovan J, et al. The landscape of somatic copy-number alteration across human cancers. Nature 2010;463: 899-905.
10. Taylor AM, Shih J, Ha G, Gao GF, Zhang X, Berger AC, et al. Genomic and functional approaches to understanding cancer aneuploidy. Cancer Cell 2018;33: 676-89.e3.
11. Barr FA, Silljé HHW, Nigg EA. Polo-like kinases and the orchestration of cell division. Nat Rev Mol Cell Biol 2004;5: 429-40.
12. Archambault V, Glover DM. Polo-like kinases: conservation and divergence in their functions and regulation. Nat Rev Mol Cell Biol 2009;10: 265-75.
13. de Cárcer G, Manning G, Malumbres M. From Plk1 to Plk5: functional evolution of polo-like kinases. Cell Cycle 2011;10: 2255-62.
14. Weiß L, Efferth T. Polo-like kinase 1 as target for cancer therapy. Exp Hematol Oncol 2012;1: 38.
15. Holtrich U, Wolf G, Bräuninger A, Karn T, Böhme B, Rübsamen-Waigmann H, et al. Induction and down-regulation of PLK, a human serine/threonine kinase expressed in proliferating cells and tumors. Proc Natl Acad Sci U S A 1994;91: 1736-40.
16. Takai N, Hamanaka R, Yoshimatsu J, Miyakawa I. Polo-like kinases (Plks) and cancer. Oncogene 2005;24: 287-91.
17. Strebhardt K, Ullrich A. Targeting polo-like kinase 1 for cancer therapy. Nat Rev Cancer 2006;6: 321-30.
18. Degenhardt Y, Lampkin T. Targeting Polo-like kinase in cancer therapy. Clin Cancer Res 2010;16: 384-9.
19. Gjertsen BT, Schöffski P. Discovery and development of the Polo-like kinase inhibitor volasertib in cancer therapy. Leukemia 2015;29: 11-9.
20. Maire V, Némati F, Richardson M, Vincent-Salomon A, Tesson B, Rigaill G, et al. Polo-like kinase 1: a potential therapeutic option in combination with conventional chemotherapy for the management of patients with triple-negative breast cancer. Cancer Res 2013;73: 813-23.
21. Giordano A, Liu Y, Armeson K, Park Y, Ridinger M, Erlander M, et al. Polo-like kinase 1 (Plk1) inhibition synergizes with taxanes in triple negative breast cancer. PLoS One 2019;14: e0224420.
22. Awada A, Dumez H, Aftimos PG, Costermans J, Bartholomeus S, Forceville K, et al. Phase I trial of volasertib, a Polo-like kinase inhibitor, plus platinum agents in solid tumors: safety, pharmacokinetics and activity. Invest New Drugs 2015;33: 611-20.
23. Simmons DL, Neel BG, Stevens R, Evett G, Erikson RL. Identification of an early-growth-response gene encoding a novel putative protein kinase. Mol Cell Biol 1992;12: 4164-9.
24. Ma S, Liu MA, Yuan YLO, Erikson RL. The serum-inducible protein kinase Snk is a G1 phase polo-like kinase that is inhibited by the calcium- and integrin-binding protein CIB. Mol Cancer Res 2003;1: 376-84.
25. Warnke S, Kemmler S, Hames RS, Tsai HL, Hoffmann-Rohrer U, Fry AM, et al. Polo-like kinase-2 is required for centriole duplication in mammalian cells. Curr Biol 2004;14: 1200-7.
26. Cizmecioglu O, Warnke S, Arnold M, Duensing S, Hoffmann I. Plk2 regulated centriole duplication is dependent on its localization to the centrioles and a functional polo-box domain. Cell Cycle 2008;7: 3548-55.
27. Seeburg DP, Pak D, Sheng M. Polo-like kinases in the nervous system. Oncogene 2005;24: 292-8.
28. Draghetti C, Salvat C, Zanoguera F, Curchod ML, Vignaud C, Peixoto H, et al. Functional whole-genome analysis identifies Polo-like kinase 2 and poliovirus receptor as essential for neuronal differentiation upstream of the negative regulator alphaB-crystallin. J Biol Chem 2009;284: 32053-65.
29. Ma S, Charron J, Erikson RL. Role of Plk2 (Snk) in mouse development and cell proliferation. Mol Cell Biol 2003;23: 6936-43.
30. Liby K, Wu H, Ouyang B, Wu S, Chen J, Dai W. Identification of the human homologue of the early-growth response gene Snk, encoding a serum-inducible kinase. DNA Seq 2001;11: 527-33.
31. Villegas E, Kabotyanski EB, Shore AN, Creighton CJ, Westbrook TF, Rosen JM. Plk2 regulates mitotic spindle orientation and mammary gland development. Development 2014;141: 1562-71.
32. Eckerdt F, Yuan J, Strebhardt K. Polo-like kinases and oncogenesis. Oncogene 2005;24: 267-76.
33. Coley HM, Hatzimichael E, Blagden S, McNeish I, Thompson A, Crook T, et al. Polo Like Kinase 2 Tumour Suppressor and cancer biomarker: new perspectives on drug sensitivity/resistance in ovarian cancer. Oncotarget 2012;3: 78-83.
34. Syed N, Smith P, Sullivan A, Spender LC, Dyer M, Karran L, et al. Transcriptional silencing of Polo-like kinase 2 (SNK/PLK2) is a frequent event in B-cell malignancies. Blood 2006;107: 250-6.
35. Benetatos L, Dasoula A, Hatzimichael E, Syed N, Voukelatou M, Dranitsaris G, et al. Polo-like kinase 2 (SNK/PLK2) is a novel epigenetically regulated gene in acute myeloid leukemia and myelodysplastic syndromes: genetic and epigenetic interactions. Ann Hematol 2011;90: 1037-45.
36. Pellegrino R, Calvisi DF, Ladu S, Ehemann V, Staniscia T, Evert M, et al. Oncogenic and tumor suppressive roles of polo-like kinases in human hepatocellular carcinoma. Hepatology 2010;51: 857-68.
37. Westbrook TF, Martin ES, Schlabach MR, Leng Y, Liang AC, Feng B, et al. A genetic screen for candidate tumor suppressors identifies REST. Cell 2005;121: 837-48.
38. Sun T, Aceto N, Meerbrey KL, Kessler JD, Zhou C, Migliaccio I, et al. Activation of multiple proto-oncogenic tyrosine kinases in breast cancer via loss of the PTPN12 phosphatase. Cell 2011;144: 703-18.
39. Weber K, Bartsch U, Stocking C, Fehse B. A multicolor panel of novel lentiviral "gene ontology" (LeGO) vectors for functional gene analysis. Mor Ther 2008;16: 698-706.
40. Knezevic J, Pfefferle AD, Petrovic I, Greene SB, Perou CM, Rosen JM. Expression of miR-200c in claudin-low breast cancer alters stem cell functionality, enhances chemosensitivity and reduces metastatic potential. Oncogene 2015;34: 5997-6006.
41. Lee OH, Kim H, He Q, Baek HJ, Yang D, Chen LY, et al. Genome-wide YFP fluorescence complementation screen identifies new regulators for telomere signaling in human cells. Mol Cell Proteomics 2011;10: M110.001628.
42. Hollern DP, Xu N, Thennavan A, Glodowski C, Garcia-Recio S, Mott KR, et al. B cells and T follicular helper cells mediate response to checkpoint inhibitors

in high mutation burden mouse models of breast cancer. Cell 2019;179: 1191-206.e21.

43. Dobin A, Davis CA, Schlesinger F, Drenkow J, Zaleski C, Jha S, et al. STAR: ultrafast universal RNA-seq aligner. Bioinformatics 2013;29: 15-21.
44. Pfefferle AD, Herschkowitz JI, Usary J, Harrell JC, Spike BT, Adams JR, et al. Transcriptomic classification of genetically engineered mouse models of breast cancer identifies human subtype counterparts. Genome Biol 2013;14: R125.
45. Johnson WE, Li C, Rabinovic A. Adjusting batch effects in microarray expression data using empirical Bayes methods. Biostatistics 2007;8: 118-27.
46. Kim IS, Gao Y, Welte T, Wang H, Liu J, Janghorban M, et al. Immuno-subtyping of breast cancer reveals distinct myeloid cell profiles and immunotherapy resistance mechanisms. Nat Cell Biol 2019;21: 1113-26.
47. Weigman VJ, Chao HH, Shabalin AA, He X, Parker JS, Nordgard SH, et al. Basal-like Breast cancer DNA copy number losses identify genes involved in genomic instability, response to therapy, and patient survival. Breast Cancer Res Treat 2012;133: 865-80.
48. Ueda A, Oikawa K, Fujita K, Ishikawa A, Sato E, Ishikawa T, et al. Therapeutic potential of PLK1 inhibition in triple-negative breast cancer. Lab Invest 2019;99: 1275-86.
49. Lu LY, Wood JL, Minter-Dykhouse K, Ye L, Saunders TL, Yu X, et al. Polo-like kinase 1 is essential for early embryonic development and tumor suppression. Mol Cell Biol 2008;28: 6870-6.
50. Matthew EM, Yen TJ, Dicker DT, Dorsey JF, Yang W, Navaraj A, et al. Replication stress, defective S-phase checkpoint and increased death in Plk2-deficient human cancer cells. Cell Cycle 2007;6: 2571-8.
51. Salvi M, Trashi E, Cozza G, Franchin C, Arrigoni G, Pinna LA. Investigation on PLK2 and PLK3 substrate recognition. Biochim Biophys Acta 2012;1824: 1366-73.
52. Park JE, Soung NK, Johmura Y, Kang YH, Liao C, Lee KH, et al. Polo-box domain: a versatile mediator of polo-like kinase function. Cell Mol Life Sci 2010;67: 1957-70.
53. Walsh EM, Shalaby A, O'Loughlin M, Keane N, Webber MJ, Kerin MJ, et al. Outcome for triple negative breast cancer in a retrospective cohort with an emphasis on response to platinum-based neoadjuvant therapy. Breast Cancer Res Treat 2019;174: 1-13.
54. Jerry DJ, Kittrell FS, Kuperwasser C, Laucirica R, Dickinson ES, Bonilla PJ, et al. A mammary-specific model demonstrates the role of the p53 tumor suppressor gene in tumor development. Oncogene 2000;19: 1052-8.
55. Pfefferle AD, Agrawal YN, Koboldt DC, Kanchi KL, Herschkowitz JI, Mardis ER, et al. Genomic profiling of murine mammary tumors identifies potential personalized drug targets for p53-deficient mammary cancers. Dis Model Mech 2016;9: 749-57.
56. Rudolph D, Steegmaier M, Hoffmann M, Grauert M, Baum A, Quant J, et al. BI 6727, a Polo-like kinase inhibitor with improved pharmacokinetic profile and broad antitumor activity. Clin Cancer Res 2009;15: 3094-102.
57. Van Loo P, Nordgard SH, Lingjærde OC, Russnes HG, Rye IH, Sun W, et al. Allele–specific copy number analysis of tumors. Proc Natl Acad Sci U S A 2010;107: 16910-5.
58. Filho OM, Stover DG, Asad S, Ansell PJ, Watson M, Loibl S, et al. Association of immunophenotype with pathologic complete response to neoadjuvant chemotherapy for triple-negative breast cancer: a secondary analysis of the BrighTNess phase 3 randomized clinical trial. JAMA Oncol 2021;7: 603-8.
59. Sun J, Wei Q, Zhou Y, Wang J, Liu Q, Xu H. A systematic analysis of FDA-approved anticancer drugs. BMC Syst Biol 2017;11: 87.
60. Petru E, Schmähl D. Cytotoxic chemotherapy-induced second primary neoplasms: clinical aspects. Neoplasma 1991;38: 147-55.
61. Liu Z, Sun Q, Wang X. PLK1, a potential target for cancer therapy. Transl Oncol 2017;10: 22-32.
62. Gutteridge REA, Ndiaye MA, Liu X, Ahmad N. Plk1 Inhibitors in Cancer Therapy: From Laboratory to Clinics. Mol Cancer Ther 2016;15: 1427-35.
63. Tian Y, Fu S, Qiu GB, Xu ZM, Liu N, Zhang XW, et al. MicroRNA-27a promotes proliferation and suppresses apoptosis by targeting PLK2 in laryngeal carcinoma. BMC Cancer 2014;14: 678.
64. Liu F, Zhang S, Zhao Z, Mao X, Huang J, Wu Z, et al. MicroRNA-27b up-regulated by human papillomavirus 16 E7 promotes proliferation and suppresses apoptosis by targeting polo-like kinase2 in cervical cancer. Oncotarget 2016;7: 19666-79.
65. Hu Z, Xu Z, Liao X, Yang X, Dong C, Luk K, et al. Polo-like kinase 2 acting as a promoter in human tumor cells with an abundance of TAp73. Onco Targets Ther 2015;8: 3475-88.
66. Ou B, Zhao J, Guan S, Wangpu X, Zhu C, Zong Y, et al. Plk2 promotes tumor growth and inhibits apoptosis by targeting Fbxw7/Cyclin E in colorectal cancer. Cancer Lett 2016;380: 457-66.
67. Matthew EM, Yang Z, Peri S, Andrake M, Dunbrack R, Ross E, et al. Plk2 loss commonly occurs in colorectal carcinomas but not adenomas: relationship to mTOR signaling. Neoplasia 2018;20: 244-55.
68. Matsumoto T, Wang PY, Ma W, Sung HJ, Matoba S, Hwang PM. Polo-like kinases mediate cell survival in mitochondrial dysfunction. Proc Natl Acad Sci U S A 2009;106: 14542-6.
69. Tavernier N, Noatynska A, Panbianco C, Martino L, Van Hove L, Schwager F, et al. Cdk1 phosphorylates SPAT-1/Bora to trigger PLK-1 activation and drive mitotic entry in C. elegans embryos. J Cell Biol 2015;208: 661-9.
70. Carbajosa S, Pansa MF, Paviolo NS, Castellaro AM, Andino DL, Nigra AD, et al. Polo-like kinase 1 inhibition as a therapeutic approach to selectively target BRCA1-deficient cancer cells by synthetic lethality induction. Clin Cancer Res 2019;25: 4049-62.
71. Muller FL, Colla S, Aquilanti E, Manzo VE, Genovese G, Lee J, et al. Passenger deletions generate therapeutic vulnerabilities in cancer. Nature 2012;488: 337-42.
72. Brabec V, Kasparkova J. Modifications of DNA by platinum complexes. Relation to resistance of tumors to platinum antitumor drugs. Drug Resist Updat 2005;8: 131-46.
73. Woods D, Turchi JJ. Chemotherapy induced DNA damage response: convergence of drugs and pathways. Cancer Biol Ther 2013;14: 379-89.
74. Settleman J, Neto JMF, Bernards R. Thinking differently about cancer treatment regimens. Cancer Discov 2021;11: 1016-23.
75. Chisamore MJ, Wilkinson HA, Flores O, Chen JD. Estrogen-related receptor-alpha antagonist inhibits both estrogen receptor-positive and estrogen receptor-negative breast tumor growth in mouse xenografts. Mol Cancer Ther 2009;8: 672-81.
76. Sabol RA, Bowles AC, Côté A, Wise R, O'Donnell B, Matossian MD, et al. Leptin produced by obesity-altered adipose stem cells promotes metastasis but not tumorigenesis of triple-negative breast cancer in orthotopic xenograft and patient-derived xenograft models. Breast Cancer Res 2019;21: 67.
77. Reddy MVR, Venkatapuram P, Mallireddigari MR, Pallela VR, Cosenza SC, Robell KA, et al. Discovery of a clinical stage multi-kinase inhibitor sodium (E)-2-{2-methoxy-5-[(2',4',6'-trimethoxystyrylsulfonyl)methyl]phenylamino}acetate (ON 01910.Na): synthesis, structure-activity relationship, and biological activity. J Med Chem 2011;54: 6254-76.
78. Jin X, Demere Z, Nair K, Ali A, Ferraro GB, Natoli T, et al. A metastasis map of human cancer cell lines. Nature 2020;588: 331-6.
79. Narvaez AJ, Ber S, Crooks A, Emery A, Hardwick B, Guarino Almeida E, et al. Modulating protein-protein interactions of the mitotic polo-like kinases to target mutant KRAS. Cell Chem Biol 2017;24: 1017-28.e7.